Organic carbon burial rate and the molybdenum proxy: Theoretical framework and application to Cenomanian-Turonian oceanic anoxic event 2

Stephen R. Meyers
Department of Geology and Geophysics, Yale University, New Haven, Connecticut, USA

Bradley B. Sageman
Department of Geological Sciences, Northwestern University, Evanston, Illinois, USA

Timothy W. Lyons
Department of Earth Sciences, University of California, Riverside, California, USA

Received 2 July 2004; revised 23 November 2004; accepted 13 December 2004; published 12 April 2005.

[1] In this study the controls on organic carbon burial and molybdenum accumulation in ancient strata are investigated through an integration of biogeochemical modeling and data analysis. Critical aspects of the study are employment of a biogeochemical model for organic matter degradation to explore the controls on pore water sulfide generation and authigenic molybdenum accumulation and use of accumulation rate data for Mo, OC, $CaCO_3$, Fe, and Ti to reconstruct organic matter remineralization processes. The model results form a conceptual framework for the interpretation of primary production estimates and geochemical burial fluxes (calculated on the basis of a high-resolution orbital timescale) for the Cenomanian-Turonian (C-T) oceanic anoxic event 2 interval in the Western Interior basin. The results of this study suggest that the strong correlation between source rock development and intervals of transgression in the geologic record (such as the C-T) could reflect a confluence of biogeochemical processes within sediments that obviates the need for large-magnitude changes in primary production levels or oceanographic conditions (such as prolonged periods of stable water column stratification).

Citation: Meyers, S. R., B. B. Sageman, and T. W. Lyons (2005), Organic carbon burial rate and the molybdenum proxy: Theoretical framework and application to Cenomanian-Turonian oceanic anoxic event 2, *Paleoceanography*, *20*, PA2002, doi:10.1029/2004PA001068.

1. Introduction

[2] The burial and preservation of organic carbon in marine sediments represents a transfer of carbon from the oxidized atmospheric reservoir (CO_2) to the reduced lithospheric reservoir (CH_2O). This process is important because it exerts a critical control on atmospheric carbon dioxide and oxygen levels over geologic time [*Berner and Canfield*, 1989; *Berner*, 1990]. Although rates of organic carbon (OC) burial have varied markedly through geologic history [e.g., *Arthur et al.*, 1985], with potentially significant climatic and environmental consequences [*Arthur et al.*, 1988; *Hayes et al.*, 1989], precise quantification of these variations and their causes has been limited by the low resolution of pre-Holocene timescales. Despite this limitation, OC burial and the formation of "black shales" have long been prominent topics of broad geologic interest. Stratigraphers, sedimentologists, paleobiologists and geochemists have focused a vast array of tools on the problem, but like most such endeavors, major debates persist in spite of significant advances in the field. Chief among these advances is a consensus that the main controls on OC burial are variations in primary production, preservation, and bulk accumulation rate [e.g., *Arthur and Sageman*, 1994; *Wignall*, 1994; *Tyson*, 1995, 2001; *Sageman and Lyons*, 2003]. At the heart of the debate, however, is the question of relative importance among these three processes [e.g., *Demaison and Moore*, 1980; *Ibach*, 1982; *Pedersen and Calvert*, 1990]. The objective of this paper is to further develop the conceptual framework for understanding major mechanisms involved in OC burial and to illuminate their relative roles.

[3] The current conceptual framework for understanding processes associated with OC burial in marine sediments is based on a body of published work that encompasses geochemical modeling studies [e.g., *Berner*, 1980; *Westrich and Berner*, 1984; *Middelburg*, 1989; *Tromp et al.*, 1995; *Tyson*, 2001], observations of modern environments and processes [e.g., *Canfield*, 1989a, 1994, 2001; *Emerson*, 1985; *Tyson and Pearson*, 1991], and analyses of geologic data from organic-rich facies [e.g., *Arthur et al.*, 1985, 1987, 1988; *Tyson and Pearson*, 1991; *Meyers et al.*, 2001; *Lyons et al.*, 2003; *Sageman et al.*, 2003]. In this study we also develop a simple geochemical model for OC burial that is based on *Berner*'s [1980] ΔG approach. We chose this approach because we believe it is accessible to the widest

0883-8305/05/2004PA001068$12.00

range of geologists who study ancient black shales, and because it specifically explores the interrelationship between OC concentration and OC reactivity (lability), factors we believe to be particularly relevant to the OC burial process. We employ the model to highlight controls on OC remineralization, we evaluate our model results in the context of selected modern observations, and ultimately we apply our new interpretative framework to better understand burial flux data from an exceptional event of ancient OC burial. The unique feature of our approach, however, is its focus on the use of molybdenum as a proxy for hydrogen sulfide (H_2S) production and thus OC decomposition during sulfate reduction.

[4] In recent years, molybdenum has emerged as a leading paleoredox indicator because of the strong correlation between OC richness and Mo concentration in many ancient black shales [e.g., *Brumsack and Thurow*, 1986; *Brumsack*, 1989; *Calvert and Pedersen*, 1993; *Jones and Manning*, 1994; *Wignall*, 1994; *Dean et al.*, 1999; *Werne et al.*, 2002; *Lyons et al.*, 2003]. Although stable isotopes of Mo are now being considered as potential recorders of global redox conditions [*Arnold et al.*, 2004], most of the focus on Mo has been limited to concentration data. Following recent advances in the study of Mo systematics [e.g., *Helz et al.*, 1996; *Zheng et al.*, 2000], we hypothesize that Mo burial flux data might provide a quantitative proxy for hydrogen sulfide production at the top of the zone of sulfate reduction and thus (indirectly) for reconstructing rates of OM remineralization by sulfate reducers in ancient OC-rich deposits. Given this relationship, the development of a geochemical model that relates primary environmental controls (e.g., variations in diluent flux, labile OM flux, total sediment burial rate, location of the upper interface of the sulfate reduction zone (SRZ), and availability of reactive iron) to rates of H_2S production constitutes a comprehensive conceptual framework for reconstruction of OC burial using the Mo proxy.

[5] Our geochemical model based on the ΔG concept (Figure 1c) is an oversimplification of the OM degradation process (Figure 1a) and is not intended to fully quantify OM remineralization [e.g., see *Tromp et al.*, 1995]. Rather, it focuses on the linkage between H_2S production and authigenic Mo deposition within the uppermost sediment layer where downward diffusion of molybdate (MoO_4^{-2}) from bottom waters would have the greatest potential to interact with H_2S produced by sulfate reducers in the sediment (Figure 1c). This relationship is central to our analysis for the following reasons. First, H_2S is perhaps the most critical biogeochemical product of OM degradation because it excludes benthic macrofauna that are the most effective agents of sediment aeration. Degree of lamination, which is a direct measure of infaunal activity, is one of the most easily observed and commonly reported parameters in ancient organic-rich facies and it appears to scale most directly to the presence/concentration of H_2S in pore and bottom waters. Second, molybdenum is a common trace metal in black shales where it tends to be enriched over modern water column values by factors of 10 to 200 or more. Molybdenum data are now available for black shales ranging in age from Precambrian to Holocene. Finally, most epicontinental black shales in the geologic record are associated with transgressions [e.g., *Arthur and Sageman*, 1994, 2005; *Wignall*, 1994] during which the flux of terrigenous constituents such as reactive iron to basinal depositional sites would have decreased. Although pyrite is a dominant component of black shales, and changes in FeS_2 abundance likely reflect changes in the rate at which H_2S was buffered within pore waters, the effect of reactive Fe availability on OM burial and Mo accumulation in black shales has not been specifically demonstrated.

[6] In addition to improving the conceptual framework for understanding OC burial, this study makes a contribution toward deconvolving the relative roles of major processes such as production, decomposition, and bulk sediment accumulation. It does so by applying knowledge gained from sensitivity experiments with our geochemical model to the interpretation of burial flux data from a well-known episode of enhanced OC burial, the Cenomanian-Turonian (C-T) boundary interval, which includes oceanic anoxic event 2 (OAE 2). The burial flux data were calculated using an orbital timescale derived from spectral analysis of the C-T study interval [*Meyers et al.*, 2001]. Use of this timescale to calculate accumulation rates for selected proxies, such as OC, $CaCO_3$, Mo, Fe, and Ti offers a unique opportunity to assess relative changes in production, preservation, and diluent accumulation that are typically quite difficult to quantify in ancient deposits. Detailed observations of sediment fabric are also used in this study to estimate relative OC preservation factors and thus improve paleoproduction estimates based on accumulation rate data for OC. Perhaps even more important, sediment fabric data reflect changes in the depth to the top of the SRZ in ancient sediments, a factor that our model experiments indicated was the most important determinant of OM remineralization rates due to sulfate reduction.

[7] In summary, the major contribution of this study lies in the power of an integrated approach to resolve the nature of OC burial in modern and ancient sediments. By incorporating insights from geochemical modeling studies with high-resolution burial flux data we develop a new proxy for OC burial that employs accumulation rate data for Mo. The study highlights a change in the consensus view of major controls on OC burial, in particular those associated with sulfate reduction, a process of fundamental importance in ancient oxygen-deficient marine settings: (1) production, preservation, and bulk accumulation rate are all important controls insofar as they influence the depth to the top of the SRZ in sediments, and thus oxygen exposure time [e.g., *Hartnett et al.*, 1998]. However, their relative importance may change over timescales of 100s of kiloyears; (2) in addition to these well-recognized controls, the role of biogeochemical buffers (i.e., reactive Fe and its influence on pore water and bottom water H_2S concentrations) must also be seriously evaluated.

2. Conceptual Framework and Geochemical Model

[8] Organic matter decomposition reactions can be approximated using first-order kinetics (first-order rate equations). Models employing such equations are useful because they provide a quantitative framework for assessing the

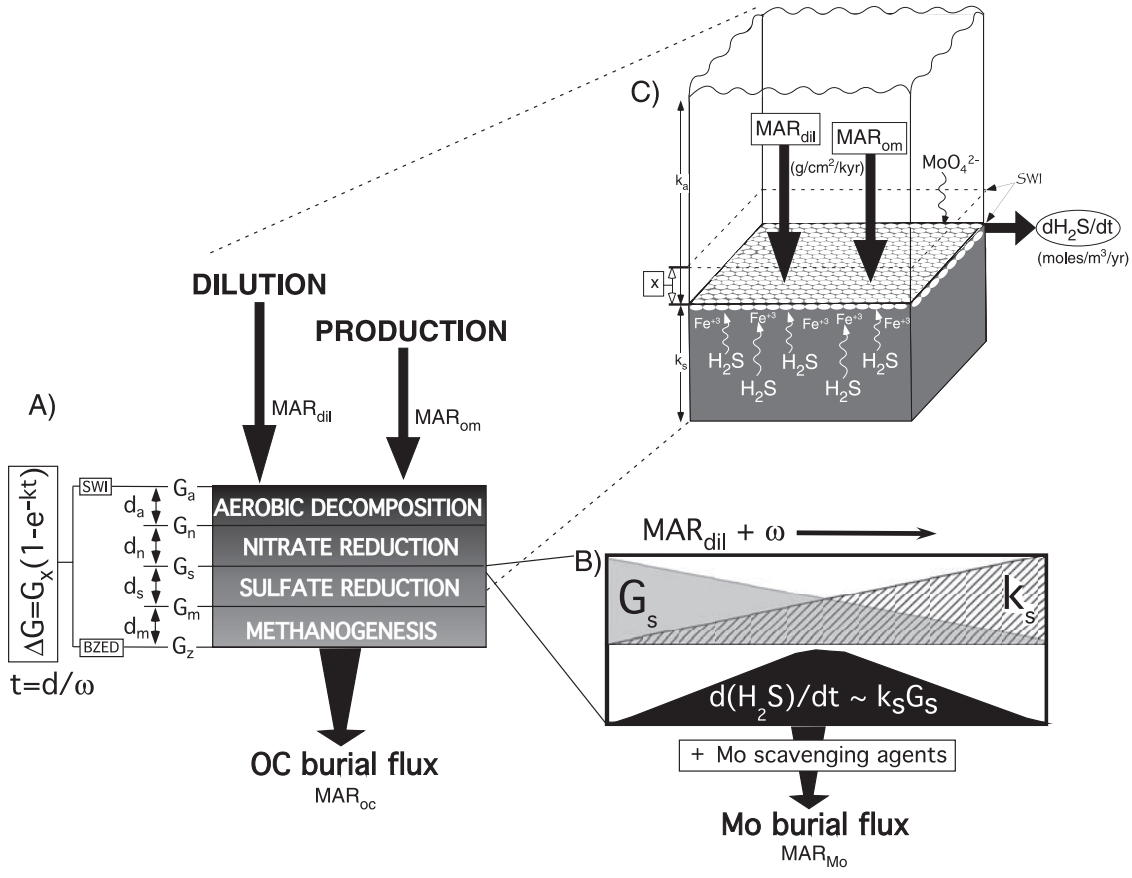

Figure 1. Theoretical model for (a) organic matter degradation in the sediment based on the ΔG model and for (b and c) the linkage between organic matter burial and molybdenum accumulation. In Figure 1a, "G" represents OC concentration at the top of each remineralization zone; G subscripts refer to aerobic decomposition (a), nitrate reduction (n), sulfate reduction (s), and methanogenesis (m); ΔG is the wt % OC change due to decomposition in each remineralization zone; ω is the bulk sedimentation rate (cm/kyr); k is the decomposition rate constant (kyr^{-1}); t is the time spent in decomposition zone (kyr); d is the thickness of decomposition zone (cm); MAR_{OC} is the organic carbon accumulation rate ($g/cm^2/kyr$); G_z is the final wt % OC; SWI is the sediment water interface; and BZED is the base of the zone of early diagenesis. In Figures 1b and 1c, G_s is the OC concentration at top of SRZ; k_s is the OC reactivity at top of SRZ; MAR_{dil} is the diluent accumulation rate ($g/cm^2/kyr$); MAR_{om} is the delivery flux of organic matter to sediment-water interface ($g/cm^2/kyr$); $d(H_2S)/dt$ is the rate of hydrogen sulfide production via sulfate reduction; MAR_{Mo} is the authigenic molybdenum accumulation ($g/cm^2/kyr$). In Figure 1c the boxed terms represents variable model inputs and the circled term represents model output; all other model parameters listed in Table 1 and Appendix B.

degree of OC degradation (ΔG; notation of *Berner* [1980]) associated with each of the major successive zones of bacterially mediated remineralization (e.g., aerobic decomposition, nitrate reduction, sulfate reduction, methanogenesis) [*Froelich et al.*, 1979] (Figure 1a). The schematic in Figure 1a illustrates a simplified form of the ΔG equation that is applied to each remineralization zone. The key variables are zone thickness ($d_{a,n,s,m}$), initial concentration of total metabolizable OC at the top of each zone ($G_{a,n,s,m}$), the average rate constant for OM decomposition within each zone ($k_{a,n,s,m}$), and sedimentation rate (ω), which together with $d_{a,n,s,m}$ dictates transit time (t) through each zone. In Figure 1a, the zonation scheme is depicted with the sediment-water interface (SWI) corresponding to the top of the zone of aerobic decomposition, but in reality this zone extends upward through the water column. Although it is possible to calculate levels of aerobic decomposition during water column transit (largely controlled by water depth; e.g., *Suess* [1980]), the ΔG model can be used to specifically explore the processes and products of OM degradation in the sediment by defining a range of OM and diluent delivery fluxes (Figure 1a). The total OC burial flux (MAR_{oc}) can be determined by the difference between initial OC concentrations resulting from given MAR_{dil} and MAR_{om} delivery fluxes and the sum of the ΔG expressions that determine the final concentration of buried OC.

[9] The ΔG approach can be used to model the rate of OC remineralization at any point in the succession shown in

Figure 1a. This rate may be expressed as $-kG$, where G is dependent upon the balance between the mass accumulation rate of OM delivered to the sediment (MAR_{om}), the mass accumulation rate of diluent (MAR_{dil}), and the degree of degradation that has occurred (ΔG). The goal of our modeling is to understand how changes in these variables might influence rates of sulfate reduction, H_2S production rates, and thus sulfide concentrations in pore waters at the top of the SRZ where G, k, and seawater molybdate availability would be greatest. As a result, our model reconstructs H_2S production rates at this level in the sediment (Figure 1c) assuming that the top of the SRZ coincides with the SWI or occurs at a known depth in the sediment. Above this depth we make the simplifying assumption that oxic degradation predominates. Although the most labile phases of organic matter are lost during transit through the water column, since burial rates are orders of magnitude less than water column transit rates, the case in which the top of the SRZ occurs above the SWI (euxinic) is essentially the same as the one in which the SRZ and the SWI are coincident.

[10] Some important conceptual relationships between G, k and sedimentation rate are illustrated in Figure 1b. Note that increases in inorganic dilution and bulk sedimentation rate result in decreased concentration (G_s) but increased reactivity (k_s) of organic matter. This occurs because higher burial rates dilute OM, but also deliver less degraded material (i.e., OM with higher k) to the SRZ. As a result of this, maximum rates of OM decomposition by sulfate reducers, maximum production of H_2S, and therefore maximum potential for Mo accumulation occurs within an intermediate range of sedimentation rates.

2.1. Authigenic Molybdenum Systematics

[11] As noted above, molybdenum enrichment has been identified as a common feature associated with OC-rich facies and oxygen-deficient environments, and a number of recent studies have been directed at understanding the controls on this process. Molybdenum occurs in low concentration in seawater and crustal rocks (<1–3 ppm) but may become authigenically enriched under sulfidic conditions and low sedimentation rates [*Emerson and Huested*, 1991; *Helz et al.*, 1996]. The enhanced accumulation of authigenic molybdenum appears to require a critical activity of hydrogen sulfide ($a_{HS^-} = 10^{-3.6}$–$10^{-4.3}$, which is equivalent to ~50–250 μM HS^-), under which molybdate (MoO_4^{-2}) may be converted to thiomolybdates ($MoO_xS(4\text{-}x)^{2-}$) and subsequently scavenged by pyrite and/or humic materials [*Helz et al.*, 1996]. Recent studies by *Zheng et al.* [2000] indicate that there may, in fact, be two critical switch points for Mo scavenging: 0.1 μM HS^- for Fe-S-Mo coprecipitation and 100 μM HS^- for Mo scavenging in the absence of pyrite. There is growing evidence to suggest that, once a switch point is achieved, Mo accumulation occurs primarily at or below the sediment water interface (via MoO_4^{-2} diffusion), even in euxinic environments (*Emerson and Huested* [1991], *Crusius et al.* [1996], *Erickson and Helz* [2000], *Zheng et al.* [2000]; see also *Lyons et al.* [2003] and *Piper and Dean* [2003] for alternative perspectives). For example, Saanich Inlet and the Black Sea, both modern euxinic settings, show absence of molybdenum enrichment in sediment trap samples but significant molybdenum enrichment below the sediment-water interface [*Francois*, 1988; *Crusius et al.*, 1996]). Similarly, *Zheng et al.*'s [2000] study of the Santa Barbara Basin indicates that ~85% of the authigenic molybdenum accumulated at or below the sediment water interface. The dominance of Mo scavenging from pore waters rather than the water column is likely due to (1) the availability of sulfide; (2) promotion of the molybdate-to-thiomolybdate conversion by Brønsted acids, which are enriched in pore waters [*Erickson and Helz*, 2000]; and (3) the high concentration of clay mineral surface sites that are available to catalyze thiomolybdate hydrolysis and sulfidation [*Vorlicek and Helz*, 2002].

[12] Achievement of the critical H_2S levels necessary for Mo accumulation from pore fluids depends on a balance between the processes that source H_2S (in situ sulfate reduction rate, as well as the rate of diffusion/advection of hydrogen sulfide into the pore water in the case of euxinic basins), the processes that deplete H_2S (the rate of formation of Fe sulfides and OM sulfurization, the rate of diffusion/advection of H_2S out of the pore water, and near-surface oxidation), and the volume of water in the connected pore space. In contrast, rates of sulfate reduction are generally unaffected by sulfate concentrations, except where sulfate levels become low [*Canfield*, 2001]. Importantly, when the rate of sulfate reduction is high, production of hydrogen sulfide can outpace depletion within pore waters (which is largely controlled by reactive Fe availability and Fe sulfide formation), and hydrogen sulfide may exceed the threshold necessary for molybdenum scavenging.

[13] On the basis of our studies, the five most important, and often interdependent, variables controlling OM concentration and average lability within the sediment SRZ, and hence the rate of H_2S production, are (1) the rate of primary production of OM; (2) the degree of OM remineralization during water column transit, which determines OM delivery flux; (3) the fluxes of inorganic diluents; (4) the location (depth) of the upper interface of the SRZ and (5) the bulk sedimentation rate (see also discussions by *Tyson* [1995], *Hedges and Keil* [1995], *Tromp et al.* [1995]). If the bulk OM is dominantly of marine photoautotrophic origin, variables (1) and (3) only affect G_s (OC concentration at the top of the SRZ), whereas variables (2), (4) and (5) affect both G_s and k_s by controlling the degree of degradation of OM that reaches the SRZ. However, variable (1) may also affect k_s if the OM delivery flux includes material derived from multiple sources (e.g., terrestrial plant biomass in addition to marine photosynthate).

[14] Data from modern settings [*Francois*, 1988; *Ravizza et al.*, 1991; *Colodner et al.*, 1995; *Crusius et al.*, 1996; *Dean et al.*, 1999; *Zheng et al.*, 2000] provide the opportunity to investigate the potential roles of these variables on molybdenum accumulation (Figure 2). Although this data set is small, it includes data from several euxinic basins, as well as from the Santa Barbara Basin, where the SRZ is perched near the SWI at some sites and is relatively deep below the SWI at other locations (based on H_2S profiles published in the work of *Zheng et al.* [2000]). Data from the Santa Barbara Basin are particularly valuable in this regard

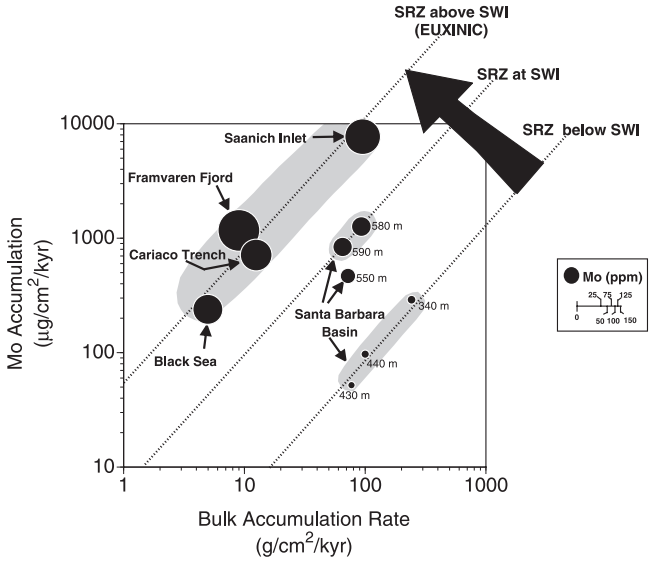

Figure 2. Bulk accumulation rate (*x* axis), molybdenum accumulation rate (*y* axis), and molybdenum concentration (bubble size) for a number of euxinic basins (Black Sea, Cariaco Trench, Framvaren Fjord, and Saanich Inlet) and the Santa Barbara Basin (data from *Zheng et al.* [2000]). SRZ is the sulfate reduction zone and SWI is the sediment water interface. See text for discussion.

because they are not influenced by differences in primary production, which is one of the potential controls on molybdenum accumulation.

[15] Molybdenum accumulation rates at the euxinic and noneuxinic settings overlap (Figure 2). However, the molybdenum and bulk sediment accumulation rates suggest three distinct fields in the cross plot (also identifiable by similar molybdenum concentrations), each of which may be qualitatively represented by lines of equivalent slope but differing y intercept. In the case of the Santa Barbara Basin sites, which have equivalent background primary production, the two lines represent distinct SRZ locations at or below the SWI. The "outlier" data point located between these two lines represents a site where hydrogen sulfide concentrations in the sediment were very low at the time of sampling (0.005 μM), but authigenic molybdenum accumulation likely occurred in the recent past when hydrogen sulfide concentrations were higher [*Zheng et al.*, 2000]. Given the negative relationship between water column depth and OM delivery for a given level of primary production [*Suess*, 1980], if OM delivery to the sediment was driving the observed patterns, the shallower sites (340 m, 440 m and 430 m) should be characterized by elevated MAR_{Mo}, which is clearly not the case. The data from the Santa Barbara Basin suggest that increased bulk accumulation rate is associated with increased molybdenum accumulation for a given SRZ location within the sediment. This relationship is consistent with the hypothesis that higher bulk accumulation rates result in more effective export of labile organic matter to the SRZ. This, in turn, drives elevated rates of hydrogen sulfide production and hence increases the potential for molybdenum scavenging.

[16] The data from euxinic sites suggest a similar slope. However, it is important to note that, in contrast to the Santa Barbara Basin, these molybdenum accumulation rates are also influenced by different levels of primary production. Regardless, the trends identified in Figure 2 underscore the importance of depth to the upper SRZ interface and bulk accumulation rate in controlling molybdenum accumulation. The three fields identified in Figure 2 also delineate three distinct molybdenum concentration zones: 0.7–1.2 ppm (SRZ below SWI), 12.9–13.6 ppm (SRZ at SWI), and >48 ppm (euxinic). We conclude that high rates of molybdenum accumulation (>100 μg/cm^2/kyr) can be achieved at low bulk accumulation rates in euxinic settings but require high bulk accumulation when the upper interface of the SRZ is deeper within the sediments. High rates are required in oxic depositional settings to bury OM rapidly below the zone of aerobic degradation and thus deliver sufficient labile OM for sulfide generation.

[17] Previous studies of sulfate reduction, such as *Canfield*'s [1989a, 1994] analyses of measured and modeled sulfate reduction rates in sediments spanning a broad range of modern depositional environments, also indicate a positive correlation between integrated sulfate reduction rate and sediment burial rate (ranging from $\sim 10^{-4}$ to $\sim 10^{1}$ g/cm^2/yr; see also *Henrichs and Reeburgh* [1987]). The positive relationship is attributable to an increase in the rate of delivery of labile organic matter to the SRZ [*Canfield*, 1989a] across gradients in depositional conditions that include variability in gross primary production and OM delivery flux to the sediment, bulk sedimentation rate, dilution of sedimented OM, and location of the sulfate reduction zone within the sediment or the water column.

2.2. Model Sensitivity Experiments

[18] To investigate the controls on H_2S production rate at the uppermost boundary of the sediment SRZ and their relationships to critical H_2S levels necessary for authigenic Mo accumulation, we developed a simple model for OM diagenesis. This model includes a sediment aerobic zone and a sulfate reduction zone. The model is graphically represented in Figure 1c. A detailed description of the model is provided in Appendix A. Specific equations employed in this model, which are adapted from similar models used by *Berner* [1980], *Tromp et al.* [1995], and *Murray and Kuivila* [1990], are listed in Appendix B. The physical and geochemical boundary conditions applied in our sensitivity experiments are listed in Table 1. The results of sensitivity experiments are presented in Figure 3. These experiments are specifically designed to delineate the relative roles of the five controls on rates of hydrogen sulfide production (outlined above) under a specific set of boundary conditions interpreted to be typical of epicontinental hemipelagic depositional settings (such as the Cretaceous Western Interior Seaway). These boundary conditions represent a much smaller range of variation in sediment burial rates (0.001 to 0.050 g/cm^2/yr) and "background" environmental conditions (e.g., production, detrital flux, etc.) than the data

Table 1. Physical and Geochemical Parameters Employed in Sensitivity Models

Parameter	Values/Expression	Source/Comments
Organic matter delivery flux (MAR_{om})	0–12.5 g/cm^2/kyr	
Diluent accumulation rate (MAR_{dil})	0–50 g/cm^2/kyr	
Sediment aerobic zone thickness (d_a)	0–5 cm	
Aerobic decomposition rate constant (k_a)	2.97 $\omega^{0.62}$	*Tromp et al.* [1995]
Sulfate reduction decomposition rate constant (k_s)	0.057 $\omega^{1.94}$	*Toth and Lerman* [1977]
Metabolizable fraction of export production (β)	0.90	*Tromp et al.* [1995]
Sediment porosity (0–10 cm depth) (ϕ)	0.80	*Berner* [1980]
Bioturbation coefficient (D_{bio})	1.0 cm^2/yr	*Tromp et al.* [1995]
Organic matter particle density	1.0 g/cm^3	
Diluent particle density	2.65 g/cm^3	intermediate between the density of silicate minerals and calcite

set compiled by *Canfield* [1989a], which represents a wide range of modern environments.

[19] Case 1 is based on a depositional setting where the upper interface of the SRZ is at or above the sediment-water interface (SWI). Figure 3a displays predicted hydrogen sulfide production rates (in moles H_2S/m^3/year) for a range of bulk sediment and OM delivery fluxes. This experiment indicates that, for a constant rate of OM delivery (i.e., line A-A′ in Figure 3a and cross plot in Figure 3b), an increase in the rate of sediment burial due to increasing diluent flux (siliciclastic sediment and/or biominerals, such as skeletal components) will force an enhanced rate of H_2S production. This enhancement is the consequence of the increase in reactivity (k_s) of pelagic OM delivered to the sediment SRZ due to increasing sediment burial rate and thus decreased O_2 exposure time [*Toth and Lerman*, 1977; *Berner*, 1980]. The increase in k_s influences the H_2S production rate more dramatically than the accompanying increase in dilution of OM (decrease in G_s), which would otherwise serve to decrease H_2S production rate. Furthermore, if increases in sediment burial rate are, in part, linked to increases in OM delivery flux (line B-B′ in Figure 3a), the sensitivity of hydrogen sulfide production to sediment burial rate is even more pronounced, reaching maximum values of 1.69 moles H_2S/m^3/yr. In the absence of H_2S depletion mechanisms (e.g., diffusion and pyrite formation), the critical pore water concentration for molybdenum accumulation (assuming the minimum threshold of 0.1 μM H_2S defined by *Zheng et al.* [2000]) would be

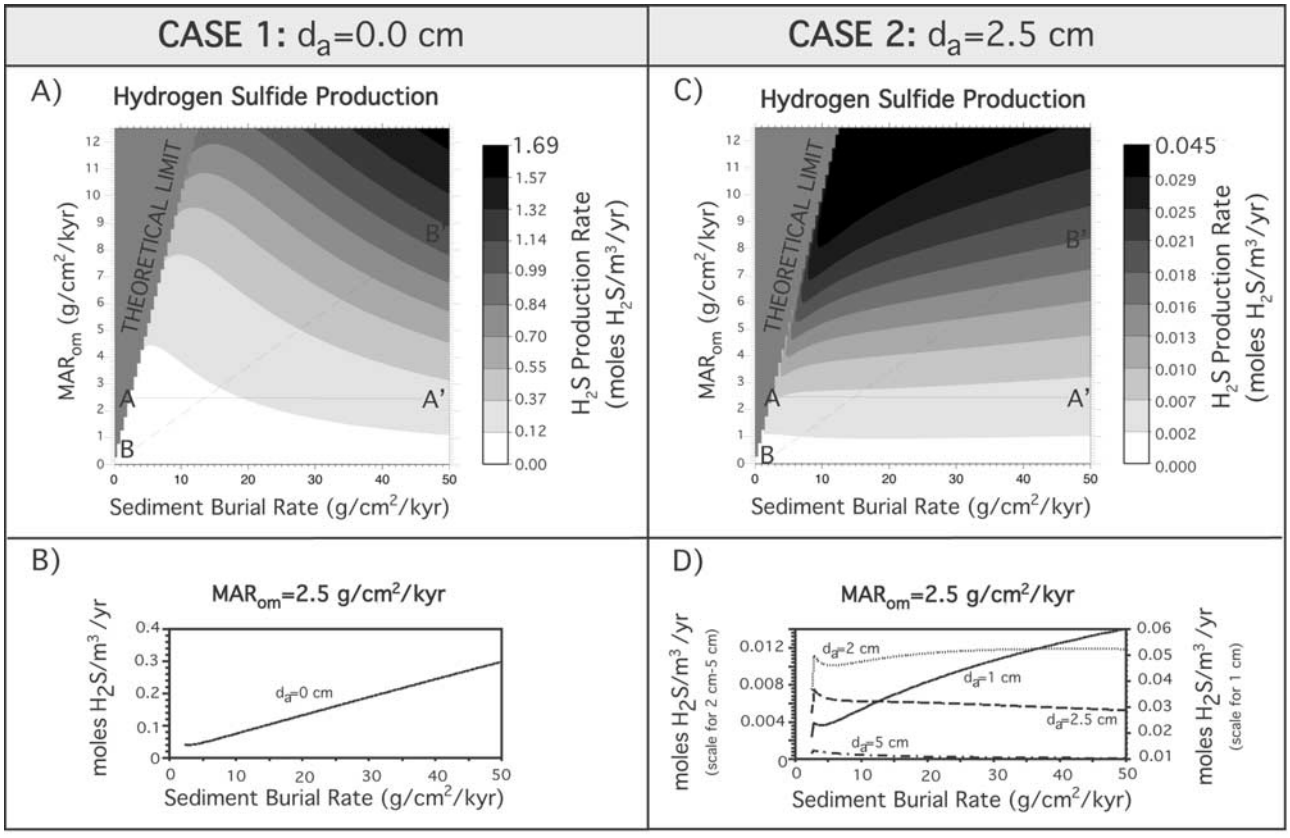

Figure 3. Output from the sensitivity experiments of the model illustrated in Figure 1c. See text and Appendix A (as well as Appendix B and Table 1) for model parameters.

achieved in a matter of hours for most of the OM delivery and sediment burial rates investigated and would be reached more rapidly as rates of burial and/or OM delivery increased.

[20] Case 2 represents a depositional setting where the upper interface of the SRZ is located 2.5 cm below the SWI. The rates of hydrogen sulfide production in this sensitivity experiment are nearly two orders of magnitude lower than in case 1, reaching a maximum value of 0.045 moles $H_2S/m^3/yr$. In contrast to case 1, the time required to achieve critical pore water H_2S concentrations for molybdenum accumulation would be one to two orders of magnitude greater for most of the investigated OM delivery and sediment burial rates, assuming absence of H_2S depletion mechanisms (i.e., even longer in the presence of reactive Fe). At low rates of OM delivery (i.e., line A-A′ in Figure 3c and cross plots in Figure 3d), an increase in sediment burial rate has little impact on the rate of hydrogen sulfide production, while at high levels of OM delivery, an increase in sediment burial rate may force a pronounced decrease in the rate of hydrogen sulfide production. However, if the change in sediment burial rate is, in part, linked to an increase in OM delivery (line B-B′ in Figure 3c), hydrogen sulfide production rate may still increase with sediment burial rate as in case 1. The results shown in case 2 also suggest that H_2S production is particularly sensitive to sediment burial at very low sediment burial rates. Figure 3d clearly displays this sensitivity and also demonstrates a progressive decrease in H_2S production rate as the thickness of the aerobic zone is increased from 1 cm to 5 cm (when OM delivery = 2.5 $g/cm^2/kyr$).

[21] In summary, these sensitivity experiments suggest that the depth of the SRZ below the SWI is the first-order control on H_2S production rate. An increase in the thickness of the sediment aerobic decomposition zone results in decreased H_2S production rates and therefore a decrease in the likelihood that hydrogen sulfide will amass to the critical level necessary for molybdenum accumulation. Changes in the rates of OM delivery and sediment burial represent important secondary controls on H_2S production rate. The rate of OM delivery shows a clear positive relationship with H_2S production rate, whereas sediment burial rate can exhibit a positive, neutral, or negative relationship with H_2S production, depending upon the magnitude of OM delivery flux and the depth of the SRZ below the SWI.

[22] Finally, it is important to note that hydrogen sulfide depletion within the pore waters of sediments (e.g., due to pyrite formation and sulfurization of OM) may balance increases in hydrogen sulfide production identified in these sensitivity models. For example, *Canfield*'s [1989b] study of modern sediments shows that iron oxides react with dissolved sulfide at a rate sufficiently high to remove sulfide as quickly as it is generated. Following sequestration of available highly reactive Fe via pyrite formation, hydrogen sulfide may accumulate in the pore waters. Sulfide depletion mechanisms such as pyrite formation may be particularly effective in countering H_2S buildup in settings with low H_2S production rates (case 2) due to the relatively large supply of un-sulfidized reactive iron from detrital iron oxides.

3. Analysis of Cenomanian-Turonian Organic Carbon Burial

3.1. Assessment of Proxy Accumulation Rates in the Bridge Creek Member

[23] Construction of high-resolution orbital timescales for ancient sedimentary deposits greatly enhances the interpretative power of biogeochemical studies by making possible calculation of burial fluxes for selected geochemical proxies [*Meyers et al.*, 2001]. Although the preservation of Milankovitch orbital cyclicity in ancient strata allows temporal resolution at timescales of 10^3–10^4 years, the applicability of cyclostratigraphic methods may be limited by the geographic and temporal extent of preserved cyclicity, as well as the quality of radiometric age control within an interval. The late Cenomanian-early Turonian (C-T) strata of the Greenhorn Formation (Bridge Creek Limestone Member) and its lateral equivalents preserve lithologic rhythmicity over 1000s of km^2 in the Western Interior Basin of North America [*Hattin*, 1985]. In the central portion of the basin this cyclicity is expressed as decimeter-scale couplets of limestone and marlstone/shale. In addition to this rhythmic lithologic variability, the interval is characterized by excellent age control based on $^{40}Ar/^{39}Ar$ dating of volcanic ashes intercalated within the rhythmic bedded sequence [*Obradovich*, 1993] and also records biogeochemical perturbations associated with widespread elevated OM burial during oceanic anoxic event 2 (OAE 2).

[24] *Gilbert* [1895] first suggested that the rhythmic deposits of the Western Interior basin could be used to construct a Cretaceous orbital timescale. Many subsequent studies have investigated the Milankovitch hypothesis in Western Interior strata [e.g., *Fischer*, 1980; *Barron et al.*, 1985; *Arthur and Dean*, 1991; *Kauffman*, 1995], culminating in quantitative confirmation of orbital signals in the C-T interval [*Sageman et al.*, 1997, 1998; *Prokoph et al.*, 2001]. Most recently, *Meyers et al.* [2001] applied a time-frequency analysis technique called evolutive harmonic analysis (EHA) to deconvolve bulk sedimentation rate changes within the C-T interval and to construct a high-resolution orbital timescale spanning OAE 2, using optical densitometry data from a core near the proposed global C-T stratotype [*Kennedy et al.*, 2000] (Figure 4). Figures 5, 6, 7, and 8 display the bulk sedimentation rate curve reconstructed by the EHA method, as well as geochemical burial flux curves calculated using weight percentage data, the EHA-derived sedimentation rate curve, and an average dry bulk density of 2.6 g/cm^3. This density value is based on an average of literature values for similar lithofacies [e.g., *Pratt*, 1985; *Bralower and Thierstein*, 1987], as well as bulk density analysis [*Wilkison and Robinson*, 2000] of samples representing lithologic variability within the study interval. The EHA method yields sedimentation rates based on application of multitaper method spectral analyses [*Thomson*, 1982] to sequential 2-m windows. Values representing 2-m moving window averages of the raw geochemical concentration data from the 1 Portland core [see

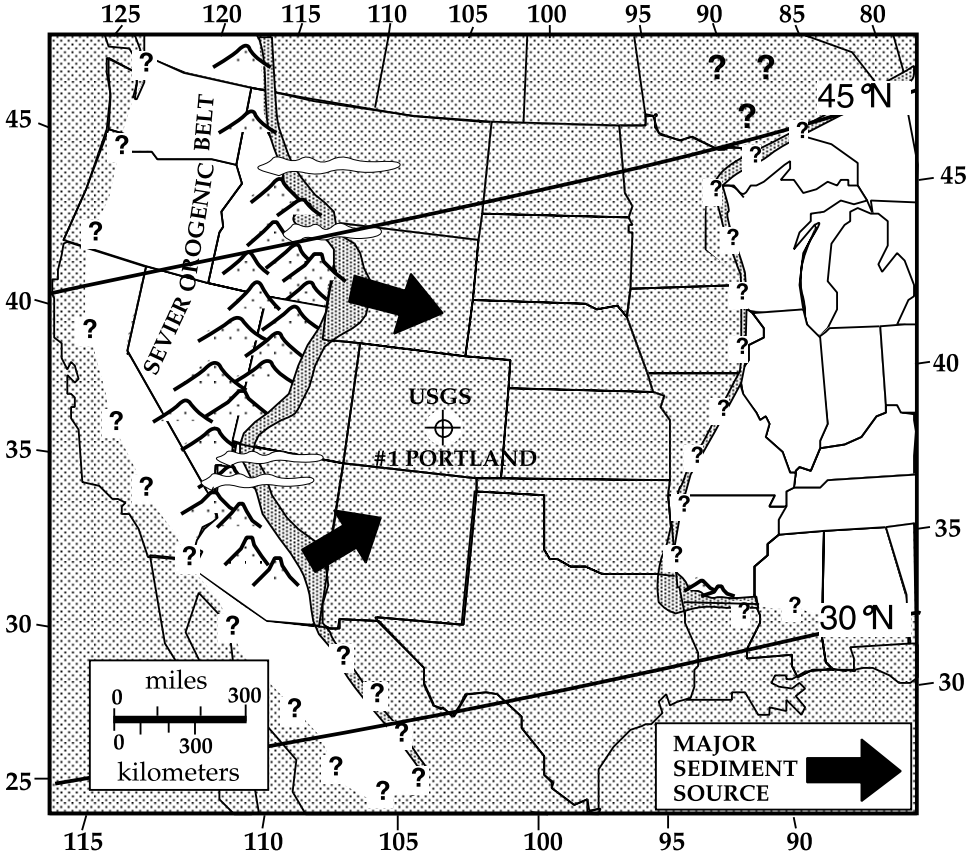

Figure 4. Paleogeographic map displaying the Western Interior seaway (early Turonian peak highstand) superimposed on a transverse mercator projection of the United States. Flooded areas are shaded, inferred boundaries are queried, and present-day latitude and longitude are displayed on the borders. Here the 30° and 45° paleolatitude lines are also shown, as well as the location of USGS 1 Portland core, the Sevier Orogenic Belt, and major sediment sources (modified from *Sageman and Arthur* [1994] and *Roberts and Kirschbaum* [1995]).

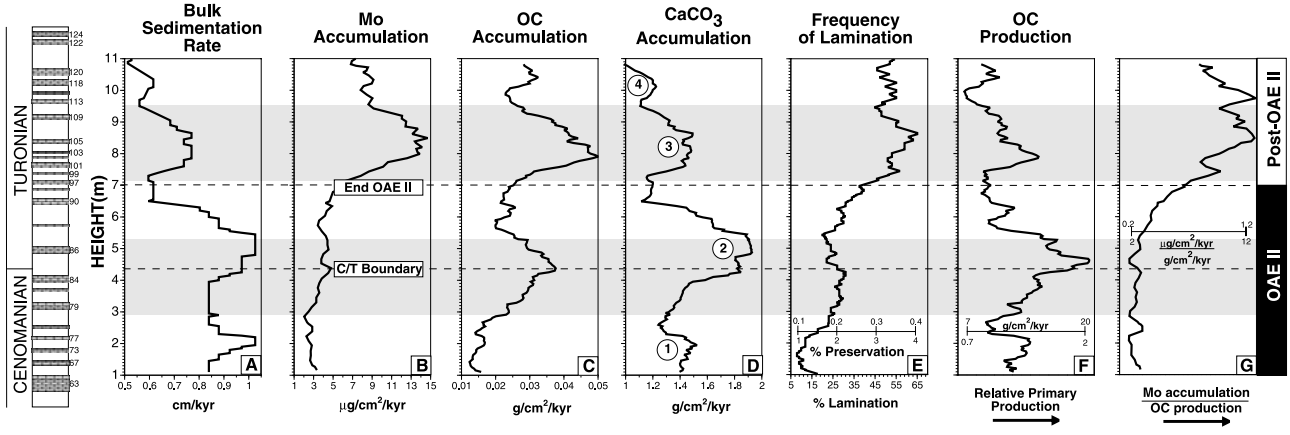

Figure 5. Geochemical proxy accumulation rates used to assess the role of paleoproductivity in the Bridge Creek Limestone Member (1 Portland core). The two shaded bands identify zones of enhanced organic carbon accumulation. Primary concentration data are illustrated in the work of *Meyers et al.* [2001] and *Sageman and Lyons* [2003]. The numbered marker limestone beds [*Cobban and Scott*, 1972] indicate correlation of the 1 Portland core to the Rock Canyon Anticline reference section.

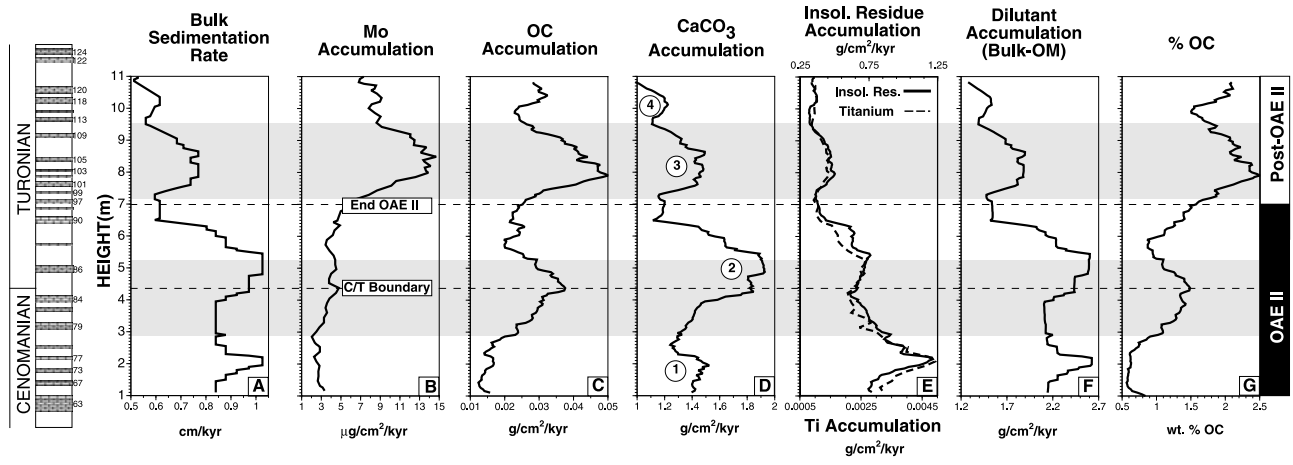

Figure 6. Geochemical proxy accumulation rates used to assess the role of dilution for the Bridge Creek Limestone Member. Primary concentration data are illustrated in the work of *Meyers et al.* [2001] and *Sageman and Lyons* [2003]. The numbered marker limestone beds [*Cobban and Scott*, 1972] indicate correlation of the 1 Portland core to the Rock Canyon Anticline reference section.

Sageman et al., 1997, 1998; *Dean and Arthur*, 1998; *Sageman and Lyons*, 2003] are therefore used to calculate the accumulation rates shown in Figures 5, 6, and 8. In addition, although changes in bulk density between shale and limestone lithologies might affect higher-resolution accumulation rate calculations, they are averaged out in the moving window approach. This method permits reconstruction of secular changes on a ±2 m scale, allowing the following trends to be identified: (1) two intervals of pronounced OC accumulation (Figure 5c, OAE 2/post-OAE 2), (2) four intervals of enhanced calcium carbonate accumulation (Figure 5d), and (3) an interval of enhanced Mo accumulation (Figure 5b, post-OAE 2).

3.2. Role of Paleoproduction

[25] Among the potential controls on OM burial, paleoproduction is one of the most challenging to estimate in studies of ancient sediments. Although it is difficult to quantify absolute levels of paleoproduction, it may be possible to constrain relative changes in production via calculation of burial fluxes for predominant biogenic components [e.g., *Bralower and Thierstein*, 1987; *Tyson*, 1995]. Two components that are potentially proportional to primary production levels in depositional systems like the Western Interior are OC and $CaCO_3$. The more commonly used method employs the accumulation rate of OC (MAR_{OC}) and an OC preservation factor [e.g., *Pratt*, 1985; *Bralower and Thierstein*, 1987; *Tyson*, 1995]. This method requires that deposited OM is dominantly sourced from pelagic photoautotrophs and that the relative degree of OC preservation can be reasonably estimated. Dominance of marine-sourced OC in the Bridge Creek Limestone Member of the central Western Interior basin has been argued previously based on organic petrographic evidence and pyrolysis data [*Pratt*, 1984], carbon isotope analyses [*Pratt*, 1985; *Arthur et al.*, 1988; *Hayes et al.*, 1989], and compound-specific organic geochemical analyses [*Pancost et al.*, 1998; *Meyers et al.*, 1999; *Simons and Kenig*, 2001]. OC preservation factors from modern settings include a range of values from ~0% to 29%, although it should be noted that most of these estimates do not fully account for diagenetic OM remineralization within the sediments [*Bralower and Thierstein*, 1987]. A reasonable preservation factor for laminated sediments that incorporates the effects of diagenetic OM remineralization in a setting like the Western Interior is assumed to be 2–4% [e.g., *Pratt*, 1985; *Bralower and Thierstein*, 1987; *Tyson*, 1995]. However, use of a constant preservation factor for the entire Bridge Creek Member would be a damaging oversimplification.

[26] As a proxy for relative changes in OC preservation during Bridge Creek deposition, we calculate changes in the frequency of lamination (FOL). FOL is calculated by applying a 2-m moving window to high-resolution (2 cm) ichnologic data (oxygen-related ichnocoenoses from *Savrda* [1998]) to determine the relative frequency of laminated intervals within each 2-m window. A doubling of the frequency of lamination in the post-OAE 2 interval (Figure 5e) is coincident with about a 40% increase in averaged hydrogen index values (average lower Bridge Creek = 235 mgHC/gOC, average upper Bridge Creek = 385 mgHC/gOC; *Pratt* [1984] and this study), and suggests an increase in the OC preservation factor [e.g., *Pratt*, 1984]. To provide an estimate of relative changes in paleoproduction (Figure 5f), we divide the MAR_{OC} estimates (Figure 5c) by their corresponding frequency of lamination, where higher FOL is inferred to represent a greater degree of OC preservation.

[27] Although speculative, it is possible to calibrate the FOL data to absolute preservation factors, which permits a quantitative estimate of paleoproduction ($gOC/cm^2/kyr$). If the FOL data are linearly scaled to preservation factors from 1 to 4%, reconstructed paleoproduction estimates range from 0.67 to 2.04 $gOC/cm^2/kyr$. These estimates are quite low relative to modern shelf settings (e.g., ~20 $gOC/cm^2/kyr$: *Tyson*, 1995). In order to produce Bridge Creek values in the range of modern shelf environments, a preservation factor on the order of 0.4% would be required. Although this value seems quite low, it is

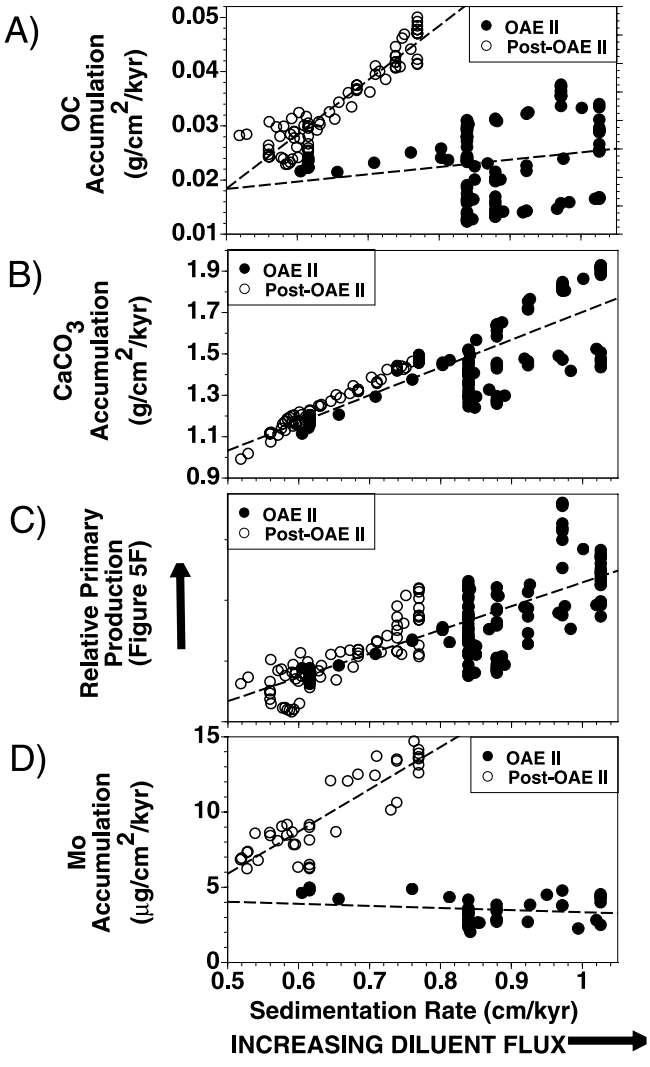

Figure 7. Cross plots of (a) MAR_{OC}, (b) MAR_{CaCO3}, (c) relative primary production, and (d) MAR_{Mo} versus sedimentation rate for the Bridge Creek Limestone. Solid circles identify data from OAE 2, and open circles identify data from the post-OAE 2 interval. Least squares regression results are indicated by dashed lines.

important to remember that the data are averaged across 2-m windows that include highly burrowed limestone facies with preservation factors that were probably much less than 1%. Most likely, the average preservation factor was somewhere between 0.4 and 4%, and paleoproduction varied between ~2 and 20 gOC/cm^2/kyr.

[28] It has been suggested that the accumulation of carbonate skeletal material, as recorded in the burial flux of calcium carbonate (MAR_{CaCO3}), may provide a proportional estimate of OM production in oceanic settings [*Brummer and Van Eijden*, 1992]. This approach is limited by a number of important caveats: (1) the composition of the phytoplankton community must not vary through time ($CaCO_3$-secreting phytoplankton must account for a constant fraction of the total production), (2) $CaCO_3$ within the rock samples must be dominantly sourced from $CaCO_3$-secreting phytoplankton (or the proportion of benthic-sourced carbonate must not change significantly), (3) the water column must be shallow enough to prevent $CaCO_3$ dissolution during transit to the SWI, and (4) there must be minimal diagenetic removal/addition of $CaCO_3$. In the case of the Bridge Creek Limestone, caveat (1) is qualitatively supported by data from *Leckie* [1985], *Leckie et al.* [1998], *Burns and Bralower* [1998], and *Li and Habib* [1996], which indicate ecological shifts in the planktic community (e.g., the "Heterohelix shift"), but no wholesale changes in the composition of the phytoplankton. In addition, *Hattin* [1975] observed that fecal pellets within basinal facies of the WIS are largely composed of coccoliths or coccolith debris, suggesting that transport of the carbonate fraction from bulk production was efficient. As for caveat (2), secular changes in the abundance of benthic shell material do occur in the Bridge Creek Limestone [*Elder*, 1989]. Although minimum abundance levels occur in association with maximum MAR_{CaCO3} values, it could be argued that dissolution explains the trend. However, this interval is also characterized by the lowest levels of benthic macrofaunal diversity and origination, and the highest levels of lamination. Whatever bias is introduced by benthic $CaCO_3$ does not appear to have obscured the trend carried by the dominant (nannofossil) input of carbonate. The shallow water column of the WIS (~300 m) satisfies caveat (3). Lastly, employment of 2-m moving averages in the MAR_{CaCO3} calculation satisfies caveat (4). Since diagenetic remineralization results in $CaCO_3$ loss from marlstones/shales and reprecipitation in adjacent limestones on scales of tens of centimeters [*Arthur et al.*, 1984; *Ricken*, 1994] we expect minimal loss within any given 2-m window. If we can assume that surface water conditions during Bridge Creek deposition remained more or less similar, MAR_{CaCO3} might provide a minimum estimate of relative changes in paleoproduction during deposition of the Bridge Creek Limestone.

[29] Interestingly, the relative changes in paleoproduction that are determined using the MAR_{OC} + preservation factor method are broadly consistent with trends in MAR_{CaCO3}, and suggest that the highest rates of OM delivery to the sediment during the C-T interval occurred in the latter part of OAE 2 (about double the post-OAE 2 level) (Figure 5). Thus both the MAR_{OC} and MAR_{CaCO3} proxies suggest that changes in primary production are not responsible for the first-order trends (OAE 2 versus post-OAE 2) in Mo or OC accumulation (i.e., Figure 5g), although there is a strong positive correlation between production, Mo and OC accumulation in the post-OAE 2 interval (Figure 5).

3.3. Role of Dilution

[30] In Figures 6 and 7 we investigate the roles of bulk sedimentation rate and inorganic dilution on OC and Mo accumulation. The two primary sources of inorganic material in the hemipelagic Bridge Creek Limestone are siliciclastic clay derived from continental runoff (the volcanogenic clay contribution is relatively minor; *Dean and Arthur* [1998]) and the pelagic carbonate flux. In general, sedimentation during deposition of the Bridge Creek Limestone was

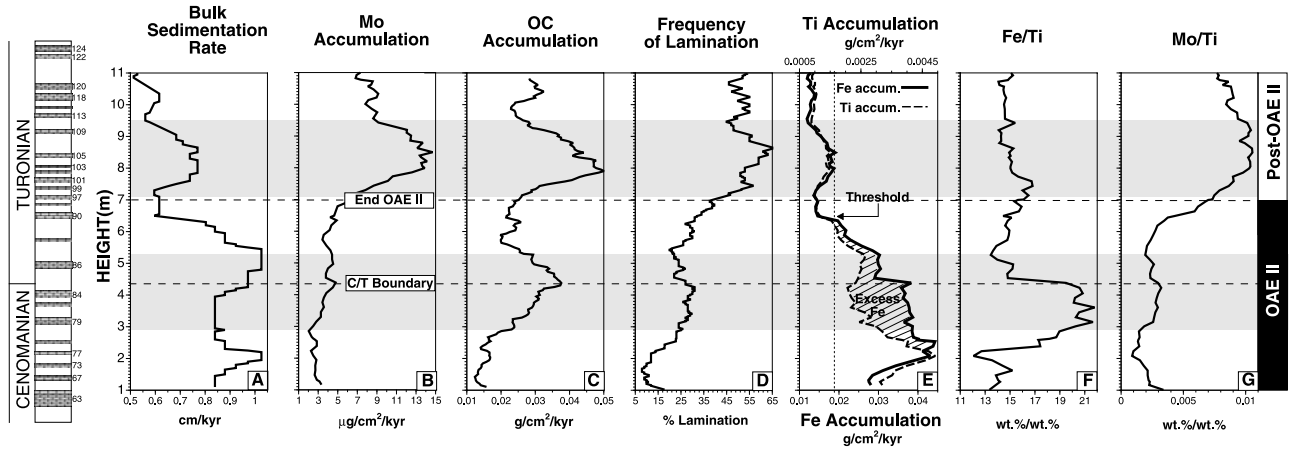

Figure 8. Geochemical proxy accumulation rates and percent lamination data from the Bridge Creek Limestone Member, used to assess location of the SRZ and iron burial fluxes. Percent lamination was calculated using the ORI rank data from *Savrda* [1998] and a 2-m moving window. Primary concentration data are illustrated in the work of *Meyers et al.* [2001] and *Sageman and Lyons* [2003]. The numbered marker limestone beds [*Cobban and Scott*, 1972] indicate correlation of the 1 Portland core to the Rock Canyon Anticline reference section.

dominated by a pelagic carbonate flux at the location of the central basin 1 Portland core (average wt %$CaCO_3$ ~70%). However, accumulation rate calculations for Ti and insoluble residue (100% − [wt %OC + wt %$CaCO_3$]) (Figure 6e) indicate variations in the contribution from siliciclastic sources during portions of OAE 2 in the lower Bridge Creek Limestone.

[31] On the basis of the diagenetic equations for OM remineralization in Appendix B, for a given rate of OM delivery and a constant remineralization regime hierarchy (i.e., the relative roles of aerobic versus anaerobic degradation), an increase in diluent flux must result in an increase in OC accumulation. This linkage between increased dilution and OC accumulation is a consequence of the dependence of degradation rate on OC concentration (−kG). Given this relationship, we would expect the OAE 2 interval (with highest sedimentation rate, production and dilution flux) to be characterized by the highest rates of OC accumulation in the Bridge Creek Limestone (Figures 6 and 7). However, the highest rates of OC accumulation occur following OAE 2, during lower sedimentation rate and thus lower diluent flux, and lower inferred paleoproduction. The cross plots in Figure 7 emphasize this dramatic change in the accumulation of the Bridge Creek geochemical proxies. Figure 7 also suggests a tight coupling of production, sedimentation rate, Mo accumulation, and OC accumulation in the post-OAE 2 interval but a decoupling of these factors during OAE 2. These results imply a fundamental difference in OM remineralization between the OAE 2 and post-OAE 2 intervals.

[32] High rates of Mo accumulation in the post-OAE 2 interval may be partially explained by elevated wt %OC (Figure 6g). If this observation can be interpreted to reflect higher initial concentrations of sedimented OM, this would have resulted in higher rates of hydrogen sulfide production and perhaps more consistent achievement of the hydrogen sulfide switch point for Mo scavenging. However, what is the ultimate cause of OC enrichment in the post-OAE 2 interval? If OM autodilution [*Tyson*, 1995] by carbonate (e.g., coccolithophore tests) is relatively consistent throughout Bridge Creek deposition, then a decrease in the siliciclastic dilution flux likely plays a key role in controlling wt %OC enrichment following OAE 2. The post-OAE 2 interval is the most condensed portion of the Bridge Creek Limestone Member, and records the peak transgression of the Greenhorn marine cycle [*Kauffman*, 1977, 1984]). Interestingly, within OAE 2 wt %OC and dilution flux (Figure 6f) are generally inversely related, although these parameters are more positively correlated in the post-OAE 2 interval. This suggests that the dilution flux primarily serves to decrease wt %OC in the OAE 2 interval, but following OAE 2, increases in dilution that would otherwise serve to decrease wt %OC are counterbalanced by a decrease in decomposition. This may be accomplished by increasing sedimentation rate and/or by shoaling of the degradational regimes within the sediment, both of which move OM through the remineralization zones more rapidly (by decreasing "t" in the model shown in Figure 1a). We can conclude that dilution mechanisms offer a partial explanation for changes in Mo burial fluxes (by increasing wt % of labile OC available for sulfate reduction), but they are not adequate to fully explain the changes in OC accumulation that were associated with enhanced Mo burial.

[33] As shown above, the change in OC accumulation between the OAE 2 and post-OAE 2 intervals cannot be fully explained as a direct consequence of changes in sedimentation rate, dilution, or production, but rather suggest a fundamental change in the rate of OM decomposition. In Figure 8, we investigate the role of SRZ location on Mo and OC accumulation. In order to resolve changes in the average depth of the upper interface of the SRZ we utilize data on the frequency of lamination described previously. We infer that changes in the degree of lamination within the study interval are a consequence of, or at least reflect, changes in the average depth of the upper interface of the

SRZ. This interpretation is corroborated by a strong correlation ($r^2 = 0.87$) between frequency of lamination and the (2-m moving average) concentration of molybdenum. A doubling of the frequency of lamination in the post-OAE 2 interval (Figure 8d) is coincident with the change to enhanced Mo and OC accumulation (Figures 8b and 8c). This suggests that shallowing of the upper interface of the SRZ and a consequent increase in the burial rate of OM into the SRZ (even under lower production rates), in other words enhanced preservation, is responsible for the first-order trends in OC and Mo accumulation within the study interval (OAE 2 versus post-OAE 2). Shallowing of the SRZ in the post-OAE 2 interval appears to be intimately linked to an overall decrease in the dilution flux, which permitted enrichment in wt %OC (G) and therefore increased rates of H_2S production. Within the post-OAE 2 regime of overall decreased dilution flux and enhanced OC concentration, increases in bulk accumulation are associated with increased wt % OC and MAR_{Mo}, suggesting enhanced preservation due to more rapid OM delivery to the sulfate reduction zone.

3.4. Linkages Between Iron and Molybdenum Burial

[34] As described earlier in the section on Mo systematics, in addition to the rate of H_2S production and the availability of Mo scavenging agents, Mo accumulation is dependent upon the rate of hydrogen sulfide removal from pore waters. The formation of authigenic iron sulfides will depress hydrogen sulfide concentrations, and pyrite is potentially an important Mo scavenging agent [*Helz et al.*, 1996]. *Dean and Arthur*'s [1989] analysis of total iron and pyrite sulfur in the Bridge Creek Limestone Member indicates that essentially all iron is in the form of pyrite (pyrite-S/total-Fe $\sim$ 1.15, the stoichiometric pyrite line). Given *Dean and Arthur*'s [1989] result, the burial flux of total iron should closely approximate pyrite iron accumulation rate throughout Bridge Creek Limestone deposition. It is worthwhile noting that this dominance of pyrite iron, or more generally, highly reactive Fe, is not typical of most modern sedimentary deposits [see *Raiswell and Canfield*, 1998].

[35] In Figure 8e, we calculate total Fe accumulation and compare the Fe burial flux to Ti accumulation (a proxy for detrital flux, which shows the same trends as insoluble residue). Figure 8e suggests that the greatest rates of pyrite accumulation occur within the OAE 2 interval. Furthermore, variations in Fe and Ti accumulation track each other within the post-OAE 2 interval but diverge within OAE 2. Divergence of the Fe and Ti accumulation rate curves during OAE 2 suggests a nondetrital reactive iron (''excess iron'') contribution during OAE 2. A mechanism for the accumulation of such excess iron has been discussed by several authors [*Raiswell and Canfield*, 1998; *Raiswell et al.*, 2001; *Wijsmans et al.*, 2001; *Lyons et al.*, 2003] and involves a dissolved iron reservoir (decoupled from local detrital flux) that is scavenged during pyrite formation in a euxinic water column. Calculation of Fe/Ti values through the study interval provides an additional parameter for assessment of this dissolved iron scavenging [*Lyons et al.*, 2003] (Figure 8f). Fe/Ti is generally greater during OAE 2 (even though the detrital Ti flux is higher), suggesting a greater degree of dissolved Fe scavenging at this time. In contrast, Mo/Ti values are enriched in the post-OAE 2 interval but are comparable to world average shale values during the time of presumed dissolved iron scavenging within OAE 2 (Figure 8g). The disagreement between Mo and Fe data (both elemental ratios and accumulation rates) is particularly curious given that dissolved Fe scavenging is believed to occur only during pyrite formation within a euxinic water column [*Lyons et al.*, 2003].

[36] This apparent contradiction may be explained by the fact that Mo accumulation requires a critical concentration of hydrogen sulfide in pore waters, whereas pyrite may form within the water column or sediments as a simple equilibrium reaction. Exhaustion or decreased influx of the ultimate reactive Fe source may have occurred following OAE 2 due to increased sea level and decreased detrital iron flux (and other factors, discussed below). Such a decrease in reactive Fe availability provides a mechanism for producing lower Fe burial fluxes and Fe/Ti values, even in a euxinic environment. The Bridge Creek burial flux data suggest that decreased availability of reactive iron following OAE 2 reduced the hydrogen-sulfide buffering capacity of the environment (via lower rates of pyrite formation), resulting in greater accumulation of H_2S and more rapid achievement of the critical level for Mo accumulation. In contrast, elevated pyrite formation likely depressed hydrogen sulfide levels in the pore waters during the OAE 2 interval, helping to inhibit Mo scavenging. The cross plot of MAR_{Mo} and MAR_{Fe} shown in Figure 9 graphically illustrates the threshold level at which decreased reactive Fe supply (as represented by the total Fe flux) serves to increase Mo accumulation.

[37] Finally, since the accumulation of authigenic iron (pyrite-Fe) is antithetic to the first-order Mo accumulation rate trend, enhanced Mo scavenging by pyrite cannot account for elevated Mo accumulation following OAE 2, as is consistent with *Lyons et al.* [2003]. According to *Zheng et al.* [2000], when sulfide concentrations rise above 100 μM, Mo accumulation may continue after Fe is completely removed from pore waters. Achievement of this concentration of hydrogen sulfide in pore waters may have contributed to the high rate of Mo accumulation in the post-OAE 2 interval.

4. Discussion

[38] In this study we employ flux data for geochemical proxies from the Bridge Creek Limestone Member to deconvolve the controls on OM burial in the central Western Interior Sea during C-T time. A key feature of our method is the use of Mo accumulation as a geochemical tracer to assess the rate of degradation of OM undergoing anaerobic metabolism by sulfate reducers. Sensitivity analysis using a geochemical model was employed to investigate the range of potential controls on Mo accumulation, each of which can be constrained using proxy burial fluxes and lithologic data. Evaluation of the Bridge Creek burial flux data with this technique suggests that OC accumulation is primarily controlled by the rate of delivery of OM to the SRZ. These

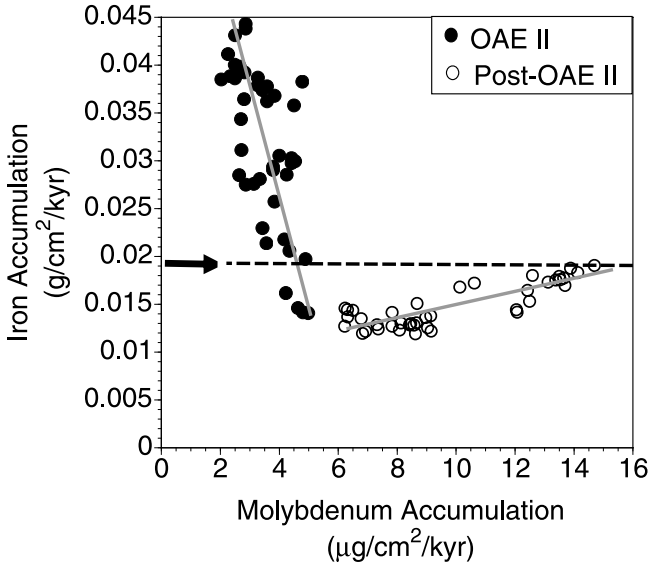

Figure 9. Cross plot of mass accumulation rate data for iron (MAR_{Fe}) and molybdenum (MAR_{Mo}) illustrates little change in MAR_{Mo} until a threshold MAR_{Fe} level is achieved, at which point Mo scavenging is enhanced and MAR_{Mo} increases rapidly for a given change in MAR_{Fe}. The threshold level of MAR_{Fe} is indicated by a dashed line.

results are consistent with *Hartnett et al.*'s [1998] study of OM burial in modern sediments, which identified an intimate linkage between oxygen exposure time and OM burial efficiency. The location of the upper boundary of the SRZ is the first-order control (OAE 2 versus post-OAE 2) on OM export into the SRZ, and elevated rates of molybdenum accumulation in the post-OAE 2 interval are a consequence of an enhanced flux of labile OM into a shallower SRZ.

[39] A key observation from the Bridge Creek data is that a preservational threshold is required for changes in production to directly impact OM burial. This preservational threshold is dictated by the rate of delivery of OM to the sulfate reduction zone, most clearly exemplified in Figure 7, which demonstrates a decoupling of sedimentation rate, MAR_{OC}, MAR_{Mo}, and MAR_{CaCO3} during OAE 2 but a tight coupling once this critical rate of OM export to the SRZ is achieved. However, what controlled the average depth of the sediment SRZ during Bridge Creek deposition?

[40] The burial flux data for the Bridge Creek suggest that the significant change in average sediment SRZ location between the OAE 2 and post-OAE 2 interval is linked to the interplay of (1) availability of reactive iron, which removes H_2S from pore water via formation of iron sulfides, and (2) degree of terrigenous (clay) dilution, which primarily serves to decrease wt% labile OC and therefore the metabolic demands associated with aerobic and anaerobic remineralization (e.g., O_2 consumption, SO_4^{2-} consumption and H_2S production). With regard to the first point, we propose that reactive Fe delivery can play a critical role in controlling depth of the redox interface within sediments, particularly in condensed hemipelagic facies. For a given OM delivery flux and MAR_{dil} flux to the SWI, a decrease in reactive Fe delivery results in faster rates of H_2S buildup in pore waters, and therefore enhanced diffusive flux of sulfide toward the SWI. This excess sulfide serves to decrease bioturbation penetration depth (via sulfide toxicity) and also functions as an oxygen sink (sulfide oxidation), which results in shoaling of the redox interface and the creation of more potential habitat for sulfate reducing bacteria (irrigation via bioturbation is required to sustain O_2 and NO_3^- in pore waters; *Berner* [1980]). Even relatively minor shoaling of the sediment SRZ (mm to cm scale) via decreased reactive Fe delivery will be amplified by a positive feedback mechanism: shoaling of the SRZ within the sediment results in higher rates of hydrogen sulfide production via increased delivery of labile OM, and therefore further shoaling of the SRZ. This mechanism is particularly effective in condensed facies because centimeter-scale changes in SRZ location can reduce OM degradation time in the aerobic zone by thousands of years, and this can increase H_2S production rate at the top of the SRZ by orders of magnitude (see models in Figure 3).

[41] The highest terrigenous reactive iron flux during Bridge Creek Limestone deposition occurred in the OAE 2 interval, and this iron source was supplemented by an additional reactive Fe source (see Figure 10 for estimates of peak fluxes). The timing of this excess (dissolved?) iron accumulation (Figure 8e) correlates with the hypothesized initiation of Tethyan oxygen minimum zone (OMZ) influence within the basin [*Leckie et al.*, 1998; *Meyers et al.*, 2001], which is also interpreted to have stimulated primary production via supplemental macronutrient (e.g., phosphorus) and/or micronutrient (e.g., iron) delivery [*Arthur et al.*, 1998; *Meyers et al.*, 2001; *Leckie et al.*, 2002; *Meyers and Sageman*, 2004]. Previous studies have suggested that excess dissolved iron during OAE 2 may be a consequence of enhanced hydrothermal activity and/or reorganization of ocean circulation [*Orth et al.*, 1993; *Sinton and Duncan*, 1997; *Kerr*, 1998; *Leckie et al.*, 2002]. Regardless of the ultimate source of reactive iron, we hypothesize that greater availability during OAE 2 enabled pyrite formation to act as a buffer in the central portion of the WIS, preventing H_2S from building-up in pore waters (<0.1 μM), even as primary production increased to its greatest levels in the later portion of OAE 2. This increase in H_2S removal during OAE 2 was accompanied by decrease in the metabolic demand associated with aerobic remineralization due to dilution of labile OC via higher terrigenous clay influx (i.e., compared to post-OAE 2). The coupling of decreased oxygen utilization and more effective H_2S buffering via pyrite formation served to increase average bioturbation penetration depth in the substrate, ultimately increasing the thickness of the aerobic decompositional zone and depressing the SRZ. These mechanisms would prevent the upper interface of the SRZ from shoaling significantly during OAE 2 and would result in lower MAR_{OC} and MAR_{Mo}. This explains why the record of OAE 2, especially its early phase (*Sciponoceras gracile* biozone), is dominated by evidence of extensive remineralization of OM compared to time equivalent sections in Europe (e.g., Eastbourne, Gubbio; *Tsikos et al.* [2004])

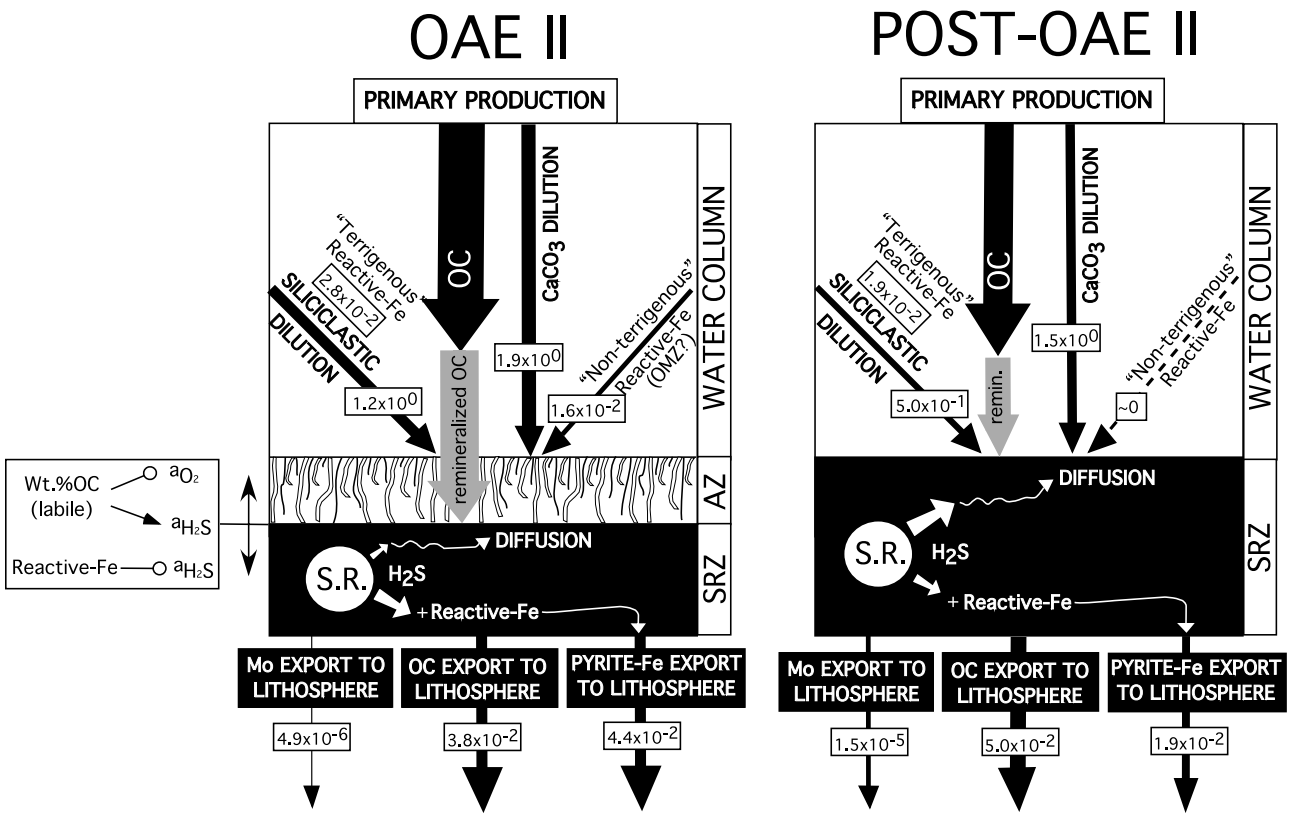

Figure 10. Schematic illustrating peak burial fluxes of siliciclastic diluent, carbonate diluent, pyrite-Fe, molybdenum, and organic carbon during OAE 2 and post-OAE 2. Quantitative estimates of reactive iron availability and qualitative estimates of primary production and average depth of the upper boundary of the SRZ are also shown. The values associated with each arrow represent fluxes in g/cm^2/kyr, and the widths of these arrows reflect the magnitude of the fluxes. The box to the left of the reconstructed fluxes depicts the positive relationship between wt % labile OC and hydrogen sulfide concentration, the negative relationship between wt % labile OC and oxygen concentration, and the negative relationship between reactive iron delivery and hydrogen sulfide concentration, all of which may influence SRZ location.

that were most likely characterized by lower reactive Fe fluxes.

[42] Shallowing of the upper interface of the SRZ in the post-OAE 2 interval can be explained as follows: First, a decrease in siliciclastic dilution associated with sea level rise to maximum transgression permitted greater wt % labile OC enrichment, which resulted in greater demand for oxygen in pore waters (via higher rates of aerobic OC remineralization) and fueled greater rates of hydrogen sulfide production, even under lower rates of primary production. The increased lability of organic matter reaching the SRZ is suggested by increased hydrogen index and MAR_{Mo} values through this interval. Second, decreased availability of reactive iron due to siliciclastic starvation and no supplementary "external" source of reactive Fe permitted the high rates of hydrogen sulfide production to overwhelm sediment pore waters. These factors resulted in enhanced Mo and OC accumulation rates following OAE 2 (Figure 10). Interestingly, once a critical preservational state was achieved via shoaling of the SRZ in the post-OAE 2 interval, increases in dilution served to increase wt.% OC, MAR_{OC} and MAR_{Mo}, suggesting that the magnitude of labile OM dilution was not sufficient to decrease the aerobic and anaerobic metabolic demand significantly within the sediments. Instead, dilution primarily served to rapidly export labile OM to the SRZ. This relationship illustrates the potential for complex interactions between organic matter reactivity (k) and concentration (G) within sediments and their impact on metabolic processes and pore water chemistry, as previously demonstrated in the sensitivity models of Figure 3.

[43] These results highlight a plausible negative feedback scenario for OC burial over geologic time: if the nutrients utilized for production are tightly linked to reactive iron delivery, an increase in production may be compensated by an increase in the degree of OM decomposition due to depletion of H_2S via pyrite formation and subsequent deepening of the upper interface of the sediment SRZ via bioturbation. Furthermore, if reactive iron delivery is primarily coupled to the terrigenous clay flux, enhanced H_2S depletion may also be associated with lower metabolic demands in the sediment, resulting in expansion of the aerobic decompositional zone and a decreased rate of H_2S production, which may accentuate deepening of the SRZ.

The burial flux data from the Bridge Creek Limestone Member suggest that the negative production-preservation feedback may be circumvented if the clay and reactive iron flux drops below a critical level (see dotted line in Figures 8e and 9). This threshold is achieved via siliciclastic cutoff, associated with relative sea level rise within the Western Interior Seaway.

[44] A linkage between reactive iron delivery and clay flux provides a viable mechanism for the creation of transgressive source rocks, even under conditions of constant or decreased levels of primary production: (1) shallowing of the sediment SRZ occurs because of high oxygen demand in the aerobic zone (decreased dilution), high H_2S production in the SRZ (decreased dilution), and low H_2S consumption (reduced reactive Fe flux) and (2) rapid export of OM into a shallow SRZ results in enhanced accumulation. This biogeochemical mechanism illustrates why condensed intervals are prone to anoxic/euxinic conditions and are generally organic-rich. The development of organic-rich sediments during OAE 2 may therefore be intimately related to an association with maximum sea level rise and highstand [*Haq et al.*, 1987; *Kauffman and Caldwell*, 1993]. Furthermore, this biogeochemical mechanism does not explicitly require a fundamental change in oceanographic conditions, such as the development of prolonged periods of stable water column stratification, and may be more consistent with the interpretation of a seasonally stratified water column increasingly proposed for shallow epicontinental basins [*Tyson and Pearson*, 1991; *Oschmann*, 1991; *Sageman and Bina*, 1997; *Murphy et al.*, 2000].

[45] Globally, the late Cenomanian-early Turonian OAE 2 interval is characterized by OC-rich, laminated black shales. The anomalously low wt %OC and burrowed character of the early OAE 2 deposits in the Western Interior can be attributed to the interplay of metabolic demand within the sediments and hydrogen sulfide depletion through reactive iron delivery and their control on the rate of OM export to the SRZ. This same mechanism may account for the apparent diachroneity in initiation of enhanced OC accumulation associated with OAE 2 at other locations.

5. Summary and Conclusions

[46] The method developed in this study employs molybdenum accumulation as a geochemical tracer to assess anaerobic metabolism. On the basis of previous theoretical and observational investigations, as well as our own modeling results and data analysis, we conclude that the primary environmental controls on sulfate reduction and molybdenum accumulation in sediments are: (1) rate of primary production of marine OM, (2) degree of water column remineralization of OM, (3) flux of inorganic diluents, (4) location of the upper interface of the SRZ, (5) bulk sedimentation rate, (6) rate of delivery of reactive iron to the SRZ, and (7) the availability of molybdenum scavenging agents. Using data from modern settings to constrain boundary conditions for a set of sensitivity experiments performed with a geochemical model, we determined that the first-order control on H_2S production rate within the sediment is the depth of the SRZ below the SWI, while OM delivery and bulk sedimentation rates represent important secondary controls. These model results suggest that hydrogen sulfide will more rapidly amass to the critical level necessary for molybdenum accumulation in settings with shallow SRZs and high rates of OM delivery, while increases in bulk sedimentation rate can exhibit a positive, neutral, or negative relationship with H_2S production depending upon the level of OM delivery and the depth of the SRZ below the SWI. Data from modern oceanic sites (e.g., Cariaco Basin, Santa Barbara Basin) support the hypothesis that SRZ location and bulk accumulation rate are significant controls on the rate of molybdenum accumulation. Subsequent analysis of burial flux data from an ancient organic carbon-rich sequence (Bridge Creek Limestone Member) within the context of the geochemical model results led to the following conclusions:

[47] 1. Organic carbon accumulation is primarily controlled by the rate of delivery of organic matter into biogeochemically mediated zones dominated by reducing conditions.

[48] 2. The location of the upper boundary of the SRZ is the first-order control (OAE 2 versus post-OAE 2) on organic matter export into the sulfate reduction zone, and processes within this zone played the dominant role in organic carbon burial during deposition of the Bridge Creek Limestone Member.

[49] 3. Change in the SRZ location between the OAE 2 and post-OAE 2 interval is attributable to the balance between metabolic demands (aerobic and anaerobic) within the sediment and hydrogen sulfide depletion through reactive iron delivery and pyrite formation.

[50] 4. A decrease in siliciclastic dilution associated with sea level rise permitted labile OC enrichment in the post-OAE 2 interval and thereby fueled greater metabolic demand, faster rates of oxygen consumption, and higher rates of hydrogen sulfide production.

[51] 5. Decreased availability of reactive iron associated with the siliciclastic cutoff in the post-OAE 2 interval enabled the high rates of hydrogen sulfide production to overwhelm sediment pore waters, resulting in shallowing of the SRZ, and enhanced Mo and OC accumulation rates.

[52] 6. Once a critical rate of export of organic matter to the SRZ is achieved (post-OAE 2), a tight coupling of production and preservation may occur.

[53] These results suggest that the development of transgressive source rocks in the geologic record may be simply explained as a consequence of siliciclastic cutoff, which concentrates labile OM and reduces the reactive iron flux, driving pore waters to a more sulfidic state. Even under lower levels of primary production, the increased rate of export of OM into a shallower SRZ will result in elevated OC accumulation rates.

Appendix A

[54] The sensitivity models displayed in Figure 3 are designed to explore the potential role of OM delivery, sediment burial rate, and depth of the upper surface of the sulfate reduction zone on the rate of hydrogen sulfide production in

sediments. These experiments employ equations (B1)–(B7) (Appendix B) to model sediment accumulation (organic matter + inorganic diluent) at the sediment water interface. Organic matter is modeled as CH_2O, with a particle density of 1 g/cm^3, and inorganic diluent is assigned a particle density of 2.65 g/cm^3 (intermediate between the density of silicate minerals and calcite; equation (B6) in Appendix B). A sediment porosity of 80% is used in these experiments, a reasonable value for sediments within 10 cm of the sediment water interface [*Berner*, 1980].

[55] We investigate OM delivery rates ranging from 0 to 12.5 g/cm^2/kyr and diluent accumulation rates from 0 to 50 g/cm^2/kyr. Given the relationship between primary production, OM delivery and water depth identified by *Suess* [1980], the maximum OM delivery rate investigated (12.5 gOM/cm^2/kyr) corresponds to primary production rates between 7.01 gOC/cm^2/kyr (water column 50 m deep) and 48.66 gOC/cm^2/kyr (water column 400 m deep), which are representative of the rates of primary production found in Holocene oceanic sites (3–50 gOC/cm^2/kyr) [*Bralower and Thierstein*, 1987]. For water columns of much greater depth, the maximum OM delivery rate investigated is not directly applicable. Similar to *Tromp et al.* [1995], organic matter is modeled as 90% metabolizable (high k) and 10% refractory (low k).

[56] Following deposition at the SWI, we employ diagenetic equations to assess remineralization via aerobic decomposition and sulfate reduction [*Berner*, 1980]. Organic matter remineralization within the aerobic decompositional zone is based on the steady state diagenetic equation for OM decomposition and redistribution (via bioturbation) within sediments [*Berner*, 1980] (equation (B8) in Appendix B). Via solution of equation (B8), the concentration of metabolizable OC (g OC/g sediment) at the base of the aerobic decompositional zone may be calculated [*Berner*, 1980; *Murray and Kuivila*, 1990] (equations (B9) and (B10) in Appendix B). In these decomposition calculations, we employ the relationship between k_a and sedimentation rate suggested by *Tromp et al.* [1995]: $k_a = 2.97\ \omega^{0.62}$. Redistribution of OM within the sediment via bioturbation is modeled with a bioturbation coefficient of 1 cm^2/year, a reasonable value for the hemipelagic settings investigated in this study [*Tromp et al.*, 1995]. Note that equation (B9) (Appendix B) differs from the simplified expression in Figure 1, due to incorporation of the role of bioturbation on OM redistribution within the sediment.

[57] Following aerobic decomposition, the rate of OC remineralization via sulfate reduction is determined by first-order kinetics (equation (B11)). In these calculations, we employ the relationship between k_s and sedimentation rate identified by *Toth and Lerman* [1977]: $k_s = 0.057\ \omega^{1.94}$. The rate of hydrogen sulfide production per unit volume of pore water (moles H_2S/cm^3/yr) is then calculated by converting the wt %OC remineralization (g OC/g sediment) to g OC/cm^3 pore water and employing the stoichiometric relationship between OC consumption and hydrogen sulfide generation (equation (B12)). The accuracy of these estimates depends upon the following approximations: (1) all wt %OC change within the decompositional zone is attributable to respiration of OC (since changes in mass associated with authigenic mineral growth are comparatively minor); (2) all OM is nondiffusible (i.e., the role of dissolved OM is minimal), and (3) sedimentation rate and compaction are invariant within the top 5 cm of the sediment. Similar approximations have been employed in previous studies [e.g., *Berner*, 1980; *Tromp et al.*, 1995]. Although more complex models may be devised, these sensitivity experiments provide a first-order approximation of hydrogen sulfide production rates in the hemipelagic settings we investigate in this study.

Appendix B: Equations Employed in Geochemical Model

[58] In this geochemical model

$$\mathrm{MAR_{om}} = \mathrm{MAR_{oc}} * \alpha \tag{B1}$$

and the empirical formula CH_2O was employed to relate organic matter to organic carbon.

$$\alpha = \frac{12.01\ \mathrm{gC/mol} + 2 * 1.008\,\mathrm{gH/mol} + 16.00\,\mathrm{gO/mol}}{12.01\,\mathrm{gC/mol}}. \tag{B2}$$

$$\mathrm{R_{burial}} = \mathrm{MAR_{om}} + \mathrm{MAR_{dil}} \tag{B3}$$

$$G_t = \frac{\mathrm{MAR_{oc}}}{\mathrm{R_{burial}}} \tag{B4}$$

$$G_a = G_t * \beta \tag{B5}$$

$$\rho = G_t\alpha * \left(1.0\,\mathrm{g/cm^3}\right) + (1 - G_t\alpha) * \left(2.65\,\mathrm{g/cm^3}\right) \tag{B6}$$

$$\omega = \frac{\mathrm{R_{burial}}}{\rho(1-\phi)} \tag{B7}$$

From *Berner* [1980]:

$$D_{bio}\left(\frac{\partial^2 G_a}{\partial x^2}\right)_t - \omega\left(\frac{\partial G_a}{\partial x}\right)_t - k_a G_a = 0 \tag{B8}$$

From *Murray and Kuivila* [1990]:

$$G_s = G_a * e^{Bx} \tag{B9}$$

From *Murray and Kuivila* [1990]:

$$B = \left(\frac{\omega - (\omega^2 + 4k_a D_{bio})^{1/2}}{2D_{bio}}\right) - \left(\frac{k_a}{D_{bio}}\right)^{1/2} \tag{B10}$$

From *Berner* [1980]:

$$\frac{dG_s}{dt} = -k_s * G_s \quad \text{(B11)}$$

From *Berner* [1980]:

$$\frac{dH_2S}{dt} = -\left(\frac{dG_s}{dt}\right)\left(\frac{\rho(1-\phi)}{\phi}\right)\left(\frac{0.5}{12.01\ \text{gC/mol}}\right) \quad \text{(B12)}$$

Notation

D_{bio} bioturbation coefficient, cm^2/yr.
dG_s/dt rate of organic matter decomposition, wt %OC/yr.
dH_2S/dt hydrogen sulfide production rate, moles $H_2S/cm^3/yr$.
G_a concentration of metabolizable organic carbon reaching sediment aerobic decompositional zone, g OC/g sediment.
G_s concentration of metabolizable organic carbon at upper surface of sediment sulfate reduction zone, g OC/g sediment.
G_t concentration of metabolizable and refractory organic carbon at sediment water interface, g OC/g sediment.
k_a first-order aerobic decomposition rate constant for metabolizable organic matter, 1/yr.
k_s first-order sulfate reduction rate constant for metabolizable organic matter, 1/yr.
MAR_{dil} diluent accumulation rate, $g/cm^2/yr$.
MAR_{oc} organic carbon delivery flux, $g/cm^2/yr$.
MAR_{om} organic matter delivery flux, $g/cm^2/yr$.
R_{burial} sediment burial rate at the sediment water interface, $g/cm^2/yr$.
t time, years.
x depth in sediment, centimeters.
α stoichiometric factor relating organic matter to organic carbon.
β fraction of total organic matter that is metabolizable.
ρ mean density of total sediment solids, g/cm^3.
ϕ sediment porosity, in volume of pore water per unit volume of total sediment (solids plus water).
ω sedimentation rate at sediment water interface, cm/yr.

[59] **Acknowledgments.** This study was funded by National Science Foundation grants EAR-0001093 (BBS), as well as by grants EAR-9875961 and EAR-0230097 (TWL). The authors acknowledge W. Dean and M. Arthur and the USGS Core Research Center, Denver Federal Center, for the contribution of samples from the USGS 1 Portland core. We also thank A. Lerman, F. Mackenzie, R. Tyson, and an anonymous reviewer for constructive criticism of the manuscript.

References

Arnold, G. L., A. D. Anbar, J. Barling, and T. W. Lyons (2004), Molybdenum isotope evidence for widespread anoxia in mid-Proterozoic oceans, *Science*, *304*, 87–90.

Arthur, M. A., and W. E. Dean (1991), A holistic geochemical approach to cyclomania; examples from Cretaceous pelagic limestone sequences, in *Cycles and Events in Stratigraphy*, edited by G. Einsele et al., pp. 126–166, Springer, New York.

Arthur, M. A., and B. B. Sageman (1994), Marine black shales: Depositional mechanisms and environments of ancient deposits, *Annu. Rev. Earth Planet. Sci.*, *22*, 499–551.

Arthur, M. A., and B. B. Sageman (2005), Sea level control on source rock development: Perspectives from the Holocene Black Sea, the mid-Cretaceous Western Interior Basin of North America, and the Late Devonian Appalachian Basin, in *The Deposition of Organic Carbon-Rich Sediments: Models, Mechanisms and Consequences*, edited by N. B. Harris, pp. 35–59, Soc. for Sediment. Geol., Tulsa, Okla.

Arthur, M. A., W. E. Dean, D. Bottjer, and P. A. Scholle (1984), Rhythmic bedding in Mesozoic-Cenozoic pelagic carbonate sequences; the primary and diagenetic origin of Milankovitch-like cycles, in *Milankovitch and Climate, Part 1*, edited by A. Berger et al., pp. 191–222, Springer, New York.

Arthur, M. A., W. E. Dean, R. Pollastro, P. A. Scholle, and G. E. Claypool (1985), A comparative geochemical study of two transgressive pelagic limestone units, Cretaceous western interior basin, U.S., in *Fine-Grained Deposits and Biofacies of the Cretaceous Western Interior Seaway: Evidence of Cyclic Sedimentary Processes*, edited by L. M. Pratt et al., pp. 16–27, Soc. for Sediment. Geol., Tulsa, Okla.

Arthur, M. A., S. O. Schlanger, and H. C. Jenkyns (1987), The Cenomanian-Turonian oceanic anoxic event 2. Paleoceanographic controls on organic matter production and preservation, in *Marine Petroleum Source Rocks*, edited by J. Brooks and A. Fleet, pp. 401–420, Geol. Soc., London.

Arthur, M. A., W. E. Dean, and L. M. Pratt (1988), Geochemical and climatic effects of increased marine organic carbon burial at the Cenomanian/Turonian boundary, *Nature*, *335*, 714–717.

Arthur, M. A., B. B. Sageman, W. E. Dean, R. L. Slingerland, L. R. Kump, and T. S. White (1998), Transgression, advection of oxygen-depleted water, and eutrophication of the mid-Cretaceous Western Interior Seaway of North America, paper presented at the Annual Meeting of the Geological Society of America, Toronto, Ont., 26–29 Oct.

Barron, E. J., M. A. Arthur, and E. G. Kauffman (1985), Cretaceous rhythmic bedding sequences: A plausible link between orbital variations and climate, *Earth Planet. Sci. Lett.*, *72*, 327–340.

Berner, R. A. (1980), *Early Diagenesis: A Theoretical Approach*, 256 pp., Princeton Univ. Press, Princeton, N. J.

Berner, R. A. (1990), Atmospheric carbon dioxide levels over Phanerozoic time, *Science*, *249*, 1382–1386.

Berner, R. A., and D. E. Canfield (1989), A new model for atmospheric oxygen over Phanerozoic time, *Am. J. Sci.*, *289*, 333–361.

Bralower, T. J., and H. R. Thierstein (1987), Organic carbon and metal accumulation rates in Holocene and mid-Cretaceous sediments: Palaeoceanographic significance, in *Marine Petroleum Source Rocks*, edited by J. Brooks and A. J. Fleet, pp. 345–369, Geol. Soc., London.

Brummer, G. J. A., and A. J. M. Van Eijden (1992), "Blue-ocean" paleoproductivity estimates from pelagic carbonate mass accumulation rates, *Mar. Micropaleontol.*, *19*, 99–117.

Brumsack, H. J. (1989), Geochemistry of recent TOC-rich sediment from the Gulf of California and the Black Sea, *Geol. Rundsch.*, *78*, 851–882.

Brumsack, H. J., and J. Thurow (1986), The geochemical facies of black shales from the Cenomanian/Turonian boundary event (CTBE), in *Biogeochemistry of black Shales; Case Studies From a Workshop*, vol. 160, edited by E. T. Degens et al., pp. 247–265, Mitt. aus dem Geol.-Palaeontol. Institut, Univ. of Hamburg, Hamburg, Germany.

Burns, C. E., and T. J. Bralower (1998), Upper Cretaceous nannofossil assemblages across the Western Interior Seaway: Implications for the origins of lithologic cycles in the Greenhorn and Niobrara formations, in *Stratigraphy and Paleoenvironments of the Cretaceous Western Interior Seaway, U.S.A.*, edited by W. E. Dean

and M. A. Arthur, pp. 35–58, Soc. for Sediment. Geol., Tulsa, Okla.

Calvert, S. E., and T. F. Pedersen (1993), Geochemistry of Recent oxic and anoxic marine sediments: Implications for the geological record, *Mar. Geol.*, *113*, 67–88.

Canfield, D. E. (1989a), Sulfate reduction and oxic respiration in marine sediments: Implications for organic carbon preservation in euxinic sediments, *Deep Sea Res.*, *36*, 121–138.

Canfield, D. E. (1989b), Reactive iron in marine sediments, *Geochim. Cosmochim. Acta*, *53*, 619–632.

Canfield, D. E. (1994), Factors influencing organic carbon preservation in marine sediments, *Chem. Geol.*, *114*, 315–329.

Canfield, D. E. (2001), Isotope fractionation by natural populations of sulfate-reducing bacteria, *Geochim. Cosmochim. Acta*, *65*, 1117–1124.

Cobban, W. A., and G. R. Scott (1972), *Stratigraphy and Ammonite Fauna of the Graneros Shale and Greenhorn Limestone Near Pueblo, Colorado*, 108 pp., U.S Geol. Soc., Denver, Colo.

Colodner, D., J. Edmond, and E. Boyle (1995), Rhenium in the Black Sea: Comparison with molybdenum and uranium, *Earth Planet. Sci. Lett.*, *131*, 1–15.

Crusius, J., S. Calvert, T. Pedersen, and D. Sage (1996), Rhenium and molybdenum enrichments in sediments as indicators of oxic, suboxic, and sulfidic conditions of deposition, *Earth Planet. Sci. Lett.*, *145*, 65–78.

Dean, W. E., and M. A. Arthur (1989), Iron-sulfur-carbon relationships in organic-carbon-rich sequences I: Cretaceous Western Interior Seaway, *Am. J. Sci.*, *289*, 708–743.

Dean, W. E., and M. A. Arthur (1998), Geochemical expression of cyclicity in Cretaceous pelagic limestone sequences: Niobrara Formation, Western Interior Seaway, in *Stratigraphy and Paleoenvironments of the Cretaceous Western Interior Seaway, U.S.A.*, edited by W. E. Dean and M. A. Arthur, pp. 227–255, Soc. for Sediment. Geol., Tulsa, Okla.

Dean, W. E., D. Z. Piper, and L. C. Peterson (1999), Molybdenum accumulation in Cariaco basin sediment over the past 24 k.y.: A record of water-column anoxia and climate, *Geology*, *27*, 507–510.

Demaison, G. J., and G. T. Moore (1980), Anoxic environments and oil source bed genesis, *Am. Assoc. Petrol. Geol. Bull.*, *64*, 1179–1209.

Elder, W. P. (1989), Molluscan extinction patterns across the Cenomanian-Turonian stage boundary in the Western Interior of the United States, *Paleobiology*, *15*, 299–320.

Emerson, S. (1985), Organic carbon preservation in marine sediments, in *The Carbon Cycle and Atmospheric CO_2: Natural Variations Archean to Present*, edited by E. T. Sunquist and W. S. Broecker, pp. 78–87, AGU, Washington, D. C.

Emerson, S. R., and S. S. Huested (1991), Ocean anoxia and the concentrations of molybdenum and vanadium in seawater, *Mar. Chem.*, *34*, 177–196.

Erickson, B. E., and G. R. Helz (2000), Molybdenum (VI) speciation in sulfidic waters: Stability and lability of thiomolybdates, *Geochim. Cosmochim. Acta*, *64*, 1149–1158.

Fischer, A. G. (1980), Gilbert-bedding rhythms and geochronology, in *The Scientific Ideas of G. K. Gilbert*, edited by E. I. Yochelson, pp. 93–104, Geol. Soc. of Am., Boulder, Colo.

Francois, R. (1988), A study on the regulation of the concentrations of some trace metals (Rb, Sr, Zn, Pb, Cu, V, Cr, Ni, Mn and Mo) in Saanich Inlet sediments, British Columbia, *Mar. Geol.*, *83*, 285–308.

Froelich, P. N., G. P. Klinkhammer, M. L. Bender, N. A. Luedtke, G. R. Heath, D. Cullen, P. Dauphin, D. Hammond, B. Hartman, and V. Maynard (1979), Early oxidation of organic matter in pelagic sediments of the eastern equatorial Atlantic: Suboxic diagenesis, *Geochim. Cosmochim. Acta*, *43*, 1075–1090.

Gilbert, G. K. (1895), Sedimentary measurement of geologic time, *Geology*, *3*, 121–127.

Haq, B. U., J. Hardenbol, and P. R. Vail (1987), Chronology of fluctuating sea levels since the Triassic, *Science*, *235*, 1156–1167.

Hartnett, H. E., R. G. Keil, J. I. Hedges, and A. H. Devol (1998), Influence of oxygen exposure time on organic carbon preservation in continental margin sediments, *Nature*, *391*, 572–574.

Hattin, D. E. (1975), Petrology and origin of fecal pellets in upper Cretaceous strata of Kansas and Saskatchewan, *J. Sediment. Petrol.*, *45*, 686–696.

Hattin, D. E. (1985), Distribution and significance of widespread, time-parallel pelagic limestone beds in Greenhorn Limestone (upper Cretaceous) of the central Great Plains and southern Rocky Mountains, in *Fine-Grained Deposits and Biofacies of the Cretaceous Western Interior Seaway: Evidence of Cyclic Sedimentary Processes*, edited by L. M. Pratt et al., pp. 28–37, Soc. for Sediment. Geol., Tulsa, Okla.

Hayes, J. M., B. N. Popp, R. Takigiku, and M. W. Johnson (1989), An isotopic study of biogeochemical relationships between carbonates and organic matter in the Greenhorn Formation, *Geochim. Cosmochim. Acta*, *53*, 2961–2972.

Hedges, J. I., and R. G. Keil (1995), Sedimentary organic matter preservation: An assessment and speculative synthesis, *Mar. Chem.*, *49*, 81–115.

Helz, G. R., C. V. Miller, J. M. Charnock, J. F. W. Mosselmans, R. A. D. Pattrick, C. D. Garner, and D. J. Vaughan (1996), Mechanism of molybdenum removal from the sea and its concentration in black shales: EXAFS evidence, *Geochim. Cosmochim. Acta*, *60*, 3631–3642.

Henrichs, S. M., and W. S. Reeburgh (1987), Anaerobic mineralization of marine sediment organic matter: Rates and the role of anaerobic processes in the oceanic carbon economy, *J. Geomicrobiol.*, *5*, 191–237.

Ibach, L. E. J. (1982), Relationship between sedimentation rate and total organic carbon content in ancient marine sediments, *Am. Assoc. Petrol. Geol. Bull.*, *66*, 170–188.

Jones, B., and D. A. C. Manning (1994), Comparison of geochemical indices used for the interpretation of palaeoredox conditions in ancient mudstones, *Chem. Geol.*, *111*, 111–129.

Kauffman, E. G. (1977), Geological and biological overview: Western Interior Cretaceous Basin, *Mt. Geol.*, *13*, 75–99.

Kauffman, E. G. (1984), Paleobiogeography and evolutionary response dynamic in the Cretaceous Western Interior Seaway of North America, in *Jurassic-Cretaceous Biochronology and Paleogeography of North America*, edited by G. E. G. Westermann, pp. 273–306, Geol. Assoc. of Can., Toronto, Ont.

Kauffman, E. G. (1995), Global change leading to biodiversity crisis in a greenhouse world: The Cenomanian-Turonian (Cretaceous) mass extinction, in *Effects of Past Global Change on Life*, edited by S. M. Stanley, pp. 47–71, Natl. Acad. Press, Washington, D. C.

Kauffman, E. G., and W. G. E. Caldwell (1993), The Western Interior basin in space and time, in *Evolution of the Western Interior Basin*, edited by W. G. E. Caldwell and E. G. Kauffman, pp. 1–30, Geol. Assoc. of Can., Toronto, Ont.

Kennedy, W. J., I. Walaszczyk, and W. A. Cobban (2000), Pueblo, Colorado, USA, candidate global boundary stratotype section and point for the base of the Turonian stage of the Cretaceous, and for the base of the middle Turonian substage, with a revision of the Inoceramidae (Bivalvia), *Acta Geol. Polonica*, *50*, 295–334.

Kerr, A. C. (1998), Oceanic plateau formation: A cause of mass extinction and black shale deposition around the Cenomanian-Turonian boundary, *J. Geol. Soc. London*, *155*, 619–626.

Leckie, R. M. (1985), Foraminifera of the Cenomanian-Turonian boundary interval, Greenhorn Formation, Rock Canyon Anticline, Pueblo, Colorado, in *Fine-Grained Deposits and Biofacies of the Cretaceous Western Interior Seaway: Evidence of Cyclic Sedimentary Processes*, edited by L. M. Pratt et al., pp. 139–149, Soc. for Sediment. Geol., Tulsa, Okla.

Leckie, R. M., R. F. Yuretich, O. O. West, D. Finkelstein, and M. Schmidt (1998), Paleoceanography of the southwestern Western Interior sea during the time of the Cenomanian-Turonian boundary (late Cretaceous), in *Stratigraphy and Paleoenvironments of the Cretaceous Western Interior Seaway, U.S.A.*, edited by W. E. Dean and M. A. Arthur, pp. 101–126, Soc. for Sediment. Geol., Tulsa, Okla.

Leckie, R. M., T. J. Bralower, and R. Cashman (2002), Oceanic anoxic events and plankton evolution: Biotic response to tectonic forcing during the mid-Cretaceous, *Paleoceanography*, *17*(3), 1041, doi:10.1029/2001PA000623.

Li, H., and D. Habib (1996), Dinoflagellate stratigraphy and its response to sea level change in Cenomanian-Turonian sections of the Western Interior of the United States, *Palaios*, *11*, 15–30.

Lyons, T. W., J. P. Werne, D. J. Hollander, and R. W. Murray (2003), Contrasting sulfur geochemistry and Fe/Al and Mo/Al ratios across the last oxic-to-anoxic transition in the Cariaco Basin, Venezuela, *Chem. Geol.*, *195*, 131–157.

Meyers, S. R., and B. B. Sageman (2004), Detection, quantification, and significance of hiatuses in pelagic and hemipelagic strata, *Earth Planet. Sci. Lett.*, *224*, 55–72.

Meyers, S. R., B. B. Sageman, and D. J. Hollander (1999), Investigation of Milankovitch forcing and OAE 2 expression in the biomarker record of the Cretaceous Western Interior Seaway, paper presented at the Annual Meeting of the Geological Society of America, Denver, Colo., 25–28 Oct.

Meyers, S. R., B. B. Sageman, and L. A. Hinnov (2001), Integrated quantitative stratigraphy of the Cenomanian-Turonian Bridge Creek limestone member using evolutive harmonic analysis and stratigraphic modeling, *J. Sediment. Res.*, *71*, 627–643.

Middelburg, J. J. (1989), A simple rate model for organic matter decomposition in marine sediments, *Geochim. Cosmochim. Acta*, *53*, 1577–1581.

Murphy, A. E., B. B. Sageman, D. J. Hollander, T. W. Lyons, and C. E. Brett (2000), Black shale deposition and faunal overturn in the Devonian Appalachian basin: Clastic starvation, seasonal water-column mixing, and efficient biolimiting nutrient recycling, *Paleoceanography*, *15*, 280–291.

Murray, J. W., and K. M. Kuivila (1990), Organic matter diagenesis in the northeast Pacific: Transition from aerobic red clay to suboxic hemipelagic sediments, *Deep Sea Res.*, *37*, 59–80.

Obradovich, J. (1993), A Cretaceous time scale, in *Evolution of the Western Interior Basin*, edited by W. G. E. Caldwell and E. G. Kauffman, pp. 379–396, Geol. Soc. of Can., Toronto, Ont.

Orth, C. J., M. Attrep, L. R. Quintana, W. P. Elder, E. G. Kauffman, R. Diner, and T. Villamil (1993), Elemental abundance anomalies in the late Cenomanian extinction interval: A search for the source(s), *Earth Planet. Sci. Lett.*, *117*, 189–204.

Oschmann, W. (1991), Anaerobic-poikiloaerobic-aerobic: A new facies zonation for modern and ancient neritic redox facies, in *Cycles and Events in Stratigraphy*, edited by G. Einsele et al., pp. 565–571, Springer, New York.

Pancost, R. D., K. H. Freeman, and M. A. Arthur (1998), Organic geochemistry of the Cretaceous Western Interior Seaway: A trans-basinal evaluation, in *Stratigraphy and Paleoenvironments of the Cretaceous Western Interior Seaway, U.S.A.*, edited by W. E. Dean and M. A. Arthur, pp. 173–188, Soc. for Sediment. Geol., Tulsa, Okla.

Pedersen, T. F., and S. E. Calvert (1990), Anoxia vs. productivity: What controls the formation of organic-carbon-rich sediments and sedimentary rocks?, *Am. Assoc. Petrol. Geol. Bull.*, *74*, 454–466.

Piper, D. Z., and W. E. Dean (2003), Trace-element deposition in the Cariaco Basin, Venezuela Shelf, under sulfate-reducing conditions—A history of the local hydrography and global climate, 20 ka to the present, 41 pp., U.S. Geol. Soc., Reston, Va.

Pratt, L. M. (1984), Influence of paleoenvironmental factors on the preservation of organic matter in middle Cretaceous Greenhorn Formation near Pueblo, Colorado, *Am. Assoc. Petrol. Geol. Bull.*, *68*, 1146–1159.

Pratt, L. M. (1985), Isotopic studies of organic matter and carbonate in rocks of the Greenhorn marine cycle, in *Fine-Grained Deposits and Biofacies of the Cretaceous Western Interior Seaway: Evidence of Cyclic Sedimentary Processes*, edited by L. A. Pratt et al., pp. 38–48, Soc. for Sediment. Geol., Tulsa, Okla.

Prokoph, A., M. Villeneuve, F. P. Agterberg, and V. Rachold (2001), Geochronology and calibration of global Milankovitch cyclicity at the Cenomanian-Turonian boundary, *Geology*, *29*, 523–526.

Raiswell, R., and D. E. Canfield (1998), Sources of iron for pyrite formation in marine sediments, *Am. J. Sci.*, *298*, 219–245.

Raiswell, R., R. Newton, and P. B. Wignall (2001), An indicator of water-column anoxia: Resolution of biofacies variations in the Kimmeridge Clay (Upper Jurassic, U.K.), *J. Sediment. Res.*, *71*, 286–294.

Ravizza, G., K. K. Turekian, and B. J. Hay (1991), The geochemistry of rhenium and osmium in recent sediments from the Black Sea, *Geochim. Cosmochim. Acta*, *55*, 3741–3752.

Ricken, W. (1994), Complex rhythmic sedimentation related to third-order sea-level variations: Upper Cretaceous, Western Interior Basin, USA, in *Orbital Forcing and Cyclic Sequences*, edited by P. L. de Boer and D. G. Smith, pp. 167–193, Blackwell, Malden, Mass.

Roberts, L. N. R., and M. A. Kirschbaum (1995), Paleogeography of the Late Cretaceous of the Western Interior of middle North America—Coal distribution and sediment accumulation, 115 pp., U. S. Geol. Soc., Reston, Va.

Sageman, B. B., and M. A. Arthur (1994), Early Turonian paleogeographic/paleobathymetric map, Western Interior, U.S., in *Mesozoic Systems of the Rocky Mountain Region*, edited by M. Caputo et al., pp. 457–470, Soc. for Sediment. Geol., Tulsa, Okla.

Sageman, B. B., and C. Bina (1997), Diversity and species abundance patterns in Late Cenomanian black shale biofacies: Western Interior, U.S., *Palaios*, *12*, 449–466.

Sageman, B. B., and T. W. Lyons (2003), Geochemistry of fine-grained sediments and sedimentary rocks, in *Treatise on Geochemistry*, vol. 7, edited by F. Mackenzie, pp. 115–158, Elsevier, New York.

Sageman, B. B., J. Rich, M. A. Arthur, G. E. Birchfield, and W. E. Dean (1997), Evidence for Milankovitch periodicities in Cenomanian-Turonian lithologic and geochemical cycles, Western Interior U.S., *J. Sediment. Res.*, *67*, 286–301.

Sageman, B., J. Rich, C. E. Savrda, T. Bralower, M. A. Arthur, and W. E. Dean (1998), Multiple Milankovitch cycles in the Bridge Creek Limestone (Cenomanian-Turonian), Western Interior basin, in *Stratigraphy and Paleoenvironments of the Cretaceous Western Interior Seaway, U.S.A.*, edited by W. E. Dean and M. A. Arthur, pp. 153–171, Soc. for Sediment. Geol., Tulsa, Okla.

Sageman, B. B., A. E. Murphy, J. P. Werne, C. A. Ver Straeten, D. J. Hollander, and T. W. Lyons (2003), A tale of shales: The relative roles of production, decomposition, and dilution in the accumulation of organic-rich strata, middle-upper Devonian, Appalachian basin, *Chem. Geol.*, *195*, 229–273.

Savrda, C. E. (1998), Ichnology of the Bridge Creek Limestone: Evidence for temporal and spatial variations in paleo-oxygenation in the Western Interior Seaway, in *Stratigraphy and Paleoenvironments of the Cretaceous Western Interior Seaway, U.S.A.*, edited by W. E. Dean and M. A. Arthur, pp. 127–136, Soc. for Sediment. Geol., Tulsa, Okla.

Simons, D.-J. H., and F. Kenig (2001), Molecular fossil constraints on the water column structure of the Cenomanian-Turonian Western Interior Seaway, USA, *Palaeogeogr. Palaeoclimatol. Palaeoecol.*, *169*, 129–152.

Sinton, C. W., and R. A. Duncan (1997), Potential links between ocean plateau volcanism and global ocean anoxia at the Cenomanian-Turonian boundary, *Econ. Geol.*, *92*, 836–842.

Suess, E. (1980), Particulate organic carbon flux in the oceans-surface productivity and oxygen utilization, *Nature*, *288*, 260–263.

Thomson, D. J. (1982), Spectrum estimation and harmonic analysis, *Proc. IEEE*, *70*, 1055–1096.

Toth, D. J., and A. Lerman (1977), Organic matter reactivity and sedimentation rates in the ocean, *Am. J. Sci.*, *277*, 465–485.

Tromp, T. K., P. Van Cappellen, and R. M. Key (1995), A global model for the early diagenesis of organic carbon and organic phosphorus in marine sediments, *Geochim. Cosmochim. Acta*, *59*, 1259–1284.

Tsikos, H., et al. (2004), Carbon-isotope stratigraphy recorded by the Cenomanian-Turonian oceanic anoxic event: Correlation and implications based on three key localities, *J. Geol. Soc. London*, *161*, 711–719.

Tyson, R. V. (1995), *Sedimentary Organic Matter: Organic Facies and Palynofacies*, 615 pp., CRC Press, Boca Raton, Fla.

Tyson, R. V. (2001), Sedimentation rate, dilution, preservation and total organic carbon: Some results of a modelling study, *Org. Geochem.*, *32*, 333–339.

Tyson, R. V., and T. H. Pearson (1991), Modern and ancient continental shelf anoxia: An overview, in *Modern and Ancient Continental Shelf Anoxia*, edited by R. V. Tyson and T. H. Pearson, pp. 1–24, Geol. Soc., London.

Vorlicek, T. P., and G. R. Helz (2002), Catalysis by mineral surfaces: Implications for Mo geochemistry in anoxic environments, *Geochim. Cosmochim. Acta*, *66*, 3679–3692.

Werne, J. P., B. B. Sageman, T. Lyons, and D. J. Hollander (2002), An integrated assessment of a "type euxinic" deposit: Evidence for multiple controls on black shale deposition in the Middle Devonian Oatka Creek Formation, *Am. J. Sci.*, *302*, 110–143.

Westrich, J. T., and R. A. Berner (1984), The role of sedimentary organic matter in bacterial sulfate reduction; the G model tested, *Limnol. Oceanogr.*, *29*, 236–249.

Wignall, P. B. (1994), *Black Shales*, 127 pp., Oxford Univ. Press, New York.

Wijsman, J. W. M., J. J. Middelburg, and C. H. R. Heip (2001), Reactive iron in Black Sea sediments: Implications for iron cycling, *Mar. Geol.*, *172*, 167–180.

Wilkison, S. L., and M. S. Robinson (2000), Bulk density of ordinary chondrite meteorites and implications for asteroidal internal structure, *Meteorit. Planet. Sci.*, *35*, 1203–1213.

Zheng, Y., R. F. Anderson, A. van Geen, and J. Kuwabara (2000), Authigenic molybdenum formation in marine sediments: A link to pore water sulfide in the Santa Barbara Basin, *Geochim. Cosmochim. Acta*, *64*, 4165–4178.

T. W. Lyons, Department of Earth Sciences, University of California, Riverside, CA 92521-0423, USA.

S. R. Meyers, Department of Geology and Geophysics, Yale University, New Haven, CT 06511, USA. (stephen.meyers@yale.edu)

B. B. Sageman, Department of Geological Sciences, Northwestern University, Evanston, IL 60208, USA.